UNIVERSITY OF CAMBRIDGE
Department of Engineering

Self-sensing Graphene Coatings for Smart Infrastructure

Author Name: Ana-Maria Marcu
Supervisor: Abir Al-Tabbaa
Date: 27.05.2020

I hereby declare that, except where specifically indicated, the work submitted herin is my own original work.

Signed AMarcu *date* 27.05.2020

SELF-SENSING GRAPHENE COATINGS

FOR SMART INFRASTRUCTURE

Technical Abstract

by Ana-Maria Marcu
Murray Edwards College
University of Cambridge
May 2020

Supervisor: Abir Al-Tabbaa

Resilience of new and existing infrastructure is a key requirement for ensuring long service times and limited disruption to asset functionality. Damage of civil infrastructures, such as bridges and underground construction, causes annually high repair and maintenance costs, leading, in some cases, to catastrophic failure. Self-sensing graphene coatings are an alternative to conventional embedded sensors used in Structural Health Monitoring, as their intrinsic sensing capabilities rely on functionalising the cement substrate. Graphene is a single-layer carbon honeycomb lattice with excellent mechanical strength and conductivity that, deposited on non-conductive substrates, can form a sensing skin.

Self-sensing is the translation of external stimuli, such as changes in strain or damage, into the variation of an internal parameter, such as electrical conductivity. A key challenge with graphene dispersion in bulk of the cement mix, as opposed to applying it as a coating, is the large quantity of material required to reach conductivity. Therefore, coatings aim to reduce functional material quantity needed to achieve sensing performance. Linearity, sensitivity, and repeatability are performance metrics that characterise the response of the sensing component.

This thesis uses few-layer graphene ink deposited on cement paste samples and aims to tests the sensing capabilities of the resulting composite. In literature, the uniformity and resistivity of the graphene cement composite are reported crucial to the performance of the resulting sensor. The project aims to establish a suitable and reliable method for applying graphene as a coating on cement samples, define the impact of graphene coating on the uniformity and resistivity of the cement surface, and develop an experimental methodology for assessing the self-sensing capabilities of the material.

The experiments conducted followed the next procedures. First, a conductive coating was achieved through deposition of few-layer graphene inks, water-based and alcohol-based, on the cement material surface. Second, the surface morphology of the material was tested by Scanning Electron Microscopy (SEM) and the uniformity of the obtained coating characterised by Electron-Dispersive X-Ray Spectroscopy (EDX). Finally, a three-point bending experiment was set-up to test the response of the graphene-cement composite. Sheet resistance measurements were conducted using a four-probe method.

The results show that a conductive graphene coating was formed on the cementitious material substrate when 50% of the surface is covered with graphene flakes. A sheet resistance of 0.81 $k\Omega/\square$ is obtained. Water-based inks drying in a high humidity environment show improved uniformity compared to alcohol-based inks. The quantity of few-layer graphene required for an optimal coating is five layers, namely 5mL of ink, which corresponds to 5.25 mg of graphene. The sensing skin detects strains as low as $20\mu\epsilon$ and presents a linear resistance versus strain characteristic, at a constant gauge factor of 61. The graphene coating provides slight reinforcement to the cementitious material sample, with Young's Modulus increasing from 2.691 GPa to 4.63 GPa for one versus fifteen layers of applied ink.

In conclusion, through literature review, planning and experimental design, a cement coating using graphene was developed. The uniformity, resistivity and sensitivity of the resulting graphene-cement composite are characterised. Further work can be conducted on the reliability and fatigue resistance of the coating, by testing under cyclic loading.

SELF-SENSING GRAPHENE COATINGS

FOR SMART INFRASTRUCTURE

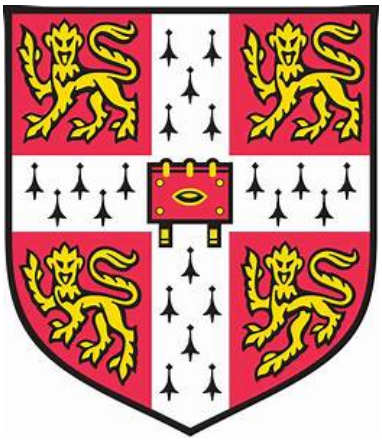

ANA-MARIA MARCU

UNIVERSITY OF CAMBRIDGE

Department of Engineering

This thesis is submitted for the degree of

MASTERS OF ENGINEERING

MAY 2020

SELF-SENSING GRAPHENE COATINGS

FOR SMART INFRASTRUCTURE

Author: ANA-MARIA MARCU

Supervisor: PROFESSOR ABIR AL-TABBAA

Advisor: PROFESSOR GOPAL MANDABUSHI

I hereby declare that this report is the result of my own work and includes nothing which is the outcome of work done in collaboration, except where specifically indicated in the text.

AMarcu

Ana-Maria Marcu, Author

27.05.2020

Date

ACKNOWLEDGMENTS

I would like to express my gratitude to everyone who provided support in writing this dissertation. Thank you to my supervisor, Professor Abir Al-Tabbaa, for her guidance and inspiration. I would like to extend my thank you to Ioanna Papanikolaou and Regana Vasanthanayagam for their support along the way. Finally, I would like to thank my family and my grandmother for their encouragement and care, as well as to my peers at University for making the small steps so much easier.

SELF-SENSING GRAPHENE COATINGS

FOR SMART INFRASTRUCTURE

Abstract

by Ana-Maria Marcu
Murray Edwards College
University of Cambridge
May 2020

Supervisor: Abir Al-Tabbaa

Infrastructure damage, especially of concrete structures, causes annually high repair and maintenance costs. Cracks in underground construction are difficult to investigate and inspect, leading to delayed intervention. Self-sensing skins are proposed as an alternative to conventional embedded systems used for Structural Health Monitoring as their intrinsic sensing capabilities rely on functional additions to the cement mix. Previous attempts at self-sensing have seen large quantities of dispersed material required inside the mix. This thesis proposes a novel graphene coating that acts as a conductive skin for continuous monitoring of cement structures. Exploiting the conductivity properties of graphene, a low quantity of material is employed for improved sensing capabilities. Few-layer graphene ink is deposited on the cement surface and its uniformity, resistivity, and self-sensing properties are investigated. The optimal coating is achieved by depositing 5.25 mg of graphene on the surface, and a linear response with a gauge factor of 61 is obtained. The research contributes to a wider effort of developing self-sensing, biomimetic materials.

Contents

List of Tables

List of Figures

Chapter One

INTRODUCTION

Infrastructure damage, especially of concrete structures, causes annually high repair and maintenance costs. Cracks in underground construction can be difficult to investigate and inspect, leading to delayed intervention. Self-sensing concrete is an alternative to conventional devices used in Structural Health Monitoring, as its intrinsic sensing capabilities rely on functional additions to the cement matrix.

1.1 Why Self-sensing?

Structural Health Monitoring (SHM) is a powerful diagnostic tool used to characterise damage in engineering structures through a combination of data acquisition, processing, and decision-making systems. Damage defines any modification that may impede the material's ability to fulfill its designated function. Applications include, but are not limited to, civil infrastructures such as bridges, buildings, and underground construction exposed to various loads throughout their lifetime which may cause damage that, in some cases, can lead to catastrophic failure. To act as a disaster mitigating tool, Structural Health Monitoring systems could ensure the precautionary detection of structural damage, prior to failure. Reliability, repeatability, and accuracy of the deployed systems are crucial for maintenance and intervention planning.

In the context of increased digitalisation, technologies employed for continuous structural health monitoring include embedded sensors, computer vision systems, unmanned aerial vehicles (drones), and sensing composites incorporated in the otherwise inert structure, which

are often referred to as self-sensing materials [29]. Embedded systems such as strain gauges, linear variable differential transducers, and accelerometers are the current state of the art for damage detection. [26]. However, a key drawback of such sensors is their inability to detect distributed damage due to their small size and point-size measurement capabilities [27]. Computer vision is an emergent technology for which the availability of low-cost cameras and improved signal processing techniques provide increased potential, but which currently is constrained by poor lighting conditions, as well as by reduced capability to sense damage prior to failure [29].

In contrast to technologies that rely on external devices for structural monitoring, self-sensing materials utilise the intrinsic capability of the composite for damage detection. [26][15] Recent developments in the field include self-reporting coatings using aggregated-induced emission luminogens (AIEGens) and microcapsules that provide a luminous colour-coded emission in response to surface deformation [23]. Carbon nanomaterials used as functional fillers in concrete have also been used for traffic monitoring [15]. Self-sensing technologies are capable of detecting deformation in a delocalised manner, which enables precise detection of damage [15]. This thesis explores further the potential of self-sensing materials in the wider context of developing biomimetic materials that self-heal and self-diagnose.

1.2 Why Graphene?

Graphene was discovered in 2004 through the micromechanical cleavage of graphite and has outstanding electrical and mechanical properties, including transparency and incredible strength. Increased interest from the academic community has been fuelled by the successful development of methods for high-yield graphene production by liquid-phase exfoliation of graphite [18]. Graphene is a two-dimensional material formed by the sp^2 bonding of carbon atoms in a hexagonal lattice. It can be stacked to obtain graphene nanoplates (GNPs), oxidised to graphene oxide (GO), and then reduced to obtain reduced graphene oxide (rGO). The carbon to oxygen ratio (C/O), number of graphene sheets in the stack, and the lateral dimension are used to create a standardised nomenclature, as shown in Figure 1.1. This

study focuses on what is described as graphite nanoplates, also referred in the literature as few-layer graphene.

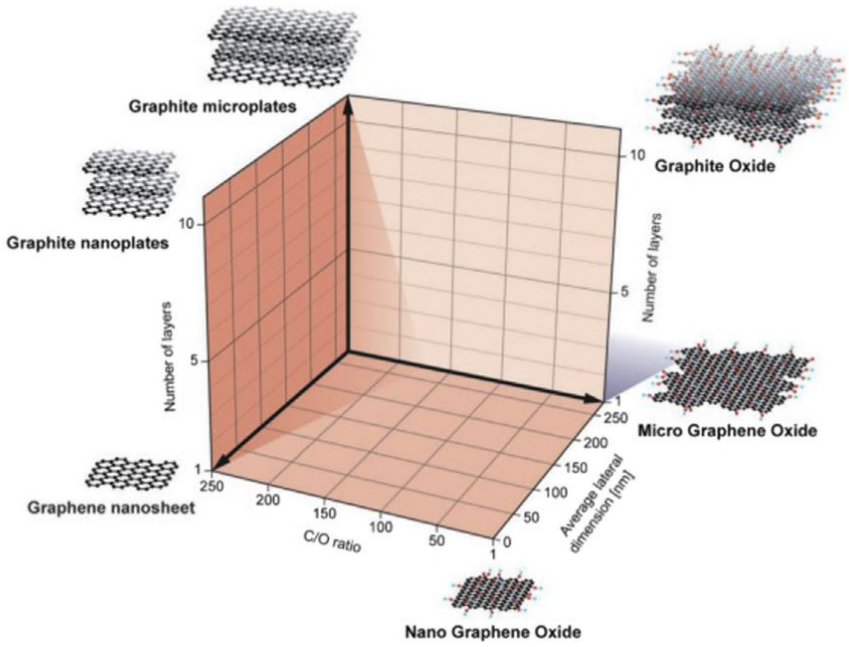

Figure 1.1 Classification of graphene-based materials based on the number of layers, the C/O ratio and the lateral dimensions [32]

The successful dispersion of graphite nanoplates into low boiling point solvents such as water and ethanol has enabled the ink-jet printing of films. [30] [19] [4]. Moreover, a review of carbon-based strain sensors shows that graphene-based materials have superior performance under low strains, as expected in concrete structures, compared to carbon nanotubes and carbon fibers. [33] Thus, this thesis aims to characterise the potential of graphite nanoplates in the context of self-sensing for cementitious materials.

1.3 Why Coatings?

Conductive coatings describe functional materials applied to the surface of a typically inert substrate to provide information on the state of the underlying element. Damage detection skins applied on the cement surface form a conductive network that modifies its properties according to deformations of the substrate. [27] In particular, for cementitious composites,

incorporation of conductive fillers in the bulk of the cement matrix has long been the focus of research. [16] However, achieving well-dispersed graphene networks inside the matrix proved a challenge due to the tendency of the functional materials to aggregate [25]. In addition, significant volumes of graphene will be required given the large volumes of concrete used. Therefore, coatings can provide an alternative to the bulk mixing of graphene elements by reducing the material quantity required without compromising on sensitivity.

1.4 Project Objectives

The overall aim of this research is to characterise graphene-cement coatings in the context of self-sensing materials. Specific objectives include:

- establish a suitable and reliable method for applying graphene as a coating on cements
- establish the impact of graphene coating on the uniformity and resistivity of the cement surface
- develop a suitable experimental methodology for assessing the self-sensing capabilities of the material
- characterise the sensitivity of the graphene-cement composite

Chapter Two

LITERATURE REVIEW

This section presents an extensive review of work done on self-sensing composites. It outlines the state of the art material on sensing technologies and identifies specific gaps in knowledge that are to be investigated further in this project.

2.1 Self-sensing

Self-sensing refers to the ability of a material to modify its intrinsic properties, such as resistance, in response to an extrinsic stimulus, such as strain, damage, or temperature. The self-sensing process comprises of two fundamental steps: functionalising the material to be responsive to external factors and measuring the resulting signal. [16]

2.1.1 Self-sensing Mechanism

The self-sensing mechanism is the mechanism for an external stimulus to be translated into an internal signal. For cementitious composites, the fractional change in resistance is used to characterise the self-sensing behaviour. The fractional change in resistance ΔR can be calculated as:

$$\Delta R = (R - R_0)/R_0$$

where R and R_0 are the initial and final electrical resistances. Self-sensing behaviour is commonly described by the gauge factor, a parameter that indicates how the resistance

changes with changes in strain. The gauge factor (GF) can be calculated as:

$$GF = \Delta R/\epsilon$$

where ϵ is the strain at which resistance R is recorded. The values of gauge factor range fromm 2 for metallic strain gauges, to 100 for piezoelectric semiconductor sensors, reaching 1100 for layer-by-layer self-assembly-formed graphene films. In concrete, the obtained strains are in the order of $\mu\epsilon$, therefore a high gauge factor is indicative of high material performance.

2.1.2 Self-sensing Materials

In recent years, many authors have attempted to increase the self-sensing capabilities of concrete by using different additions to the cement mix. [16]. In the literature, three main methods of functionalising concrete are reported. First, mixing conductive fibers inside the cement matrix leads to the formation of a conductive network that enables self-sensing properties. This approach, although extensively researched, requires large quantities of fibres mixed within the mix [25]. [16] Second, an alternative to bulk mixing has been proposed by various authors [31], [1] who suggest mixing a conductive filler or coated aggregates only in the top layer of the specimen. Effectively a conductive layer is formed at the top of the beam. A third proposed approach is to coat the cement surface without mixing it into the cement substrate [22], [14]. A summary of the attempts at functionalising concrete reported in the literature is outlined in Figure 2.1.

The response of conductive coatings subjected to three-point [27] or four-point [1] bending depends on the nature of the material used. Carbon nanotube coatings have piezoresistive properties and if embedded in a polymer matrix can also reinforce the concrete member [27] while acting as a sensing device. Carbon nanofiber paste reportedly acts as a sensing skin [1]. Figure 2.2 outlines the response of a carbon nanofiber coating subjected to a varying bending moment. The resistance of the sheet decreases with increasing compressive strain, as indicated by the increasingly negative value in the fractional change in resistance. The

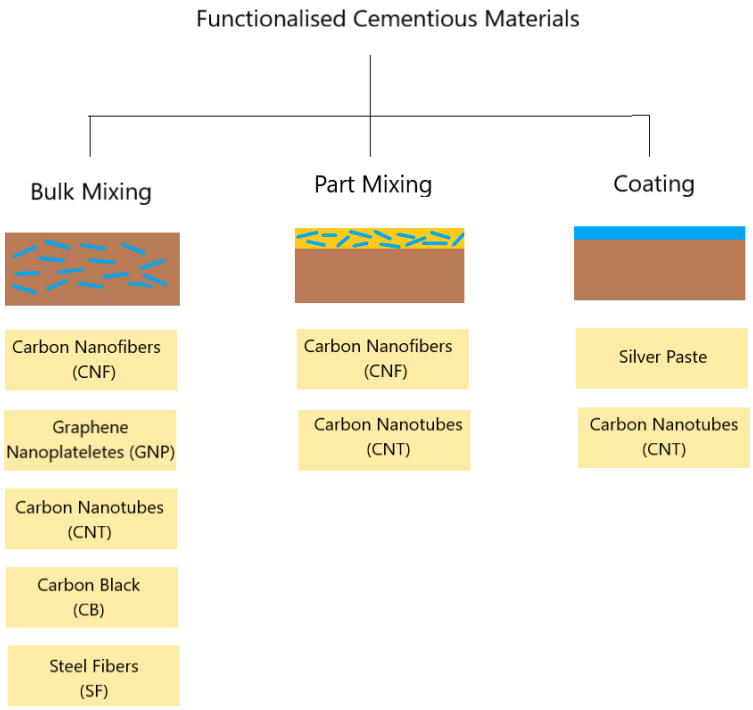

Figure 2.1 Functionalised cementitious materials for self-sensing applications

slope of the fractional change in resistance versus strain plot is the gauge factor of the sensing skin, which for this system is 198. This compares favourably to conventional metallic strain gauges that rely on mechanical deformation and have a gauge factor of 2. A nonlinear effect may be observed in the carbon nanofiber coating as the data of Figure 2.2 is better fitted by a second-order function. Thus, the choice of material for the coating element can impact the resulting response.

2.2 Graphene Coatings

Graphene is a two-dimensional material formed by planar sp^2 bonding of carbon atoms arranged in a perfect honeycomb lattice [33]. The excellent sensing capabilities of graphene are linked to its conductive and mechanical properties, including thermal conductivity in the order of 5000 W/mK, high electron mobility of 250,000 cm^2/Vs and incredible stiffness

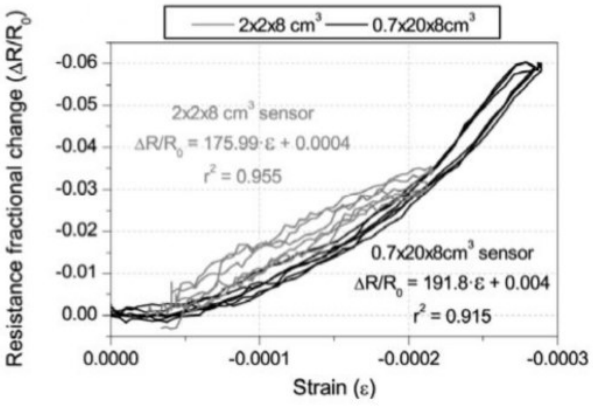

]

Figure 2.2 Strain sensing characteristic of a carbon nanofiber cementitious coating under four-point bending [1]

estimated at 1 TPa [24].

A key challenge recognised in the literature [33] [17] [4] is controlling the properties of the deposited graphene, the nature of the substrate, and the deposition process, to obtain the desired sensing capabilities, such as a high sensitivity and excellent linearity. This study exploits the properties of graphene to adapt to the cement substrate and create a sensing skin.

2.2.1 Effect of Deposition Process

Two common graphene deposition methods are outlined in the literature: wet approaches and dry approaches. Dry approaches include Chemical Vapour Deposition (CVD) [10] and direct dry transfer[33]. These methods lead to the formation of a monolayer honeycomb graphene lattice that exhibits strain sensing properties through the mechanical deformation of the hexagonal structure of graphene upon straining. Chemical Vapour Deposited graphene thin-films [10] exhibit good linearity, but their ability to measure low strains is limited by wrinkles formed in the deposition process, as shown in Figure 2.3b. Chemical-Vapour Deposited graphene was capable of measuring strains between 3%-5% [10]. Figure 2.3 shows the strain sensing response of CVD deposited graphene. In concrete applications the expected strains are in the order of $\mu\epsilon$, lower than the detection limit of CVD deposited graphene. [6] Moreover, CVD is an energy-intensive process with limited scalability. Thus, CVD may

Reference	GF	Max. Strain	Fabrication	Process	Substrate
[4]	125	1.25	Graphene Ink	Inkjet Printing	Paper
[17]	100	1.5	Graphene Ink	Spray Coating	Glass
[3]	19.3	0.66	Graphite Ink	Screen Printing	Flexible Plastic
[11]	61.5	0.05	R Graphene Oxide	Drop Casting	TiO2 composite
[10]	151	5	Graphene	CVD	PDMS
[6]	42.2	20	Graphene	Spray Coating	PDMS
[20]	1037	2	fGNanoplateletes	LbL self-assembly	PDMS
[33]	754	5	R Graphene Oxide	LbL self-assembly	PDMS

Table 2.1 Graphene strain sensors fabrication techniques [adapted from [33]]

have limited potential for concrete skins, despite its reported high sensitivity. A summary of graphene deposition techniques reviewed from literature is outlined in Table 2.1.

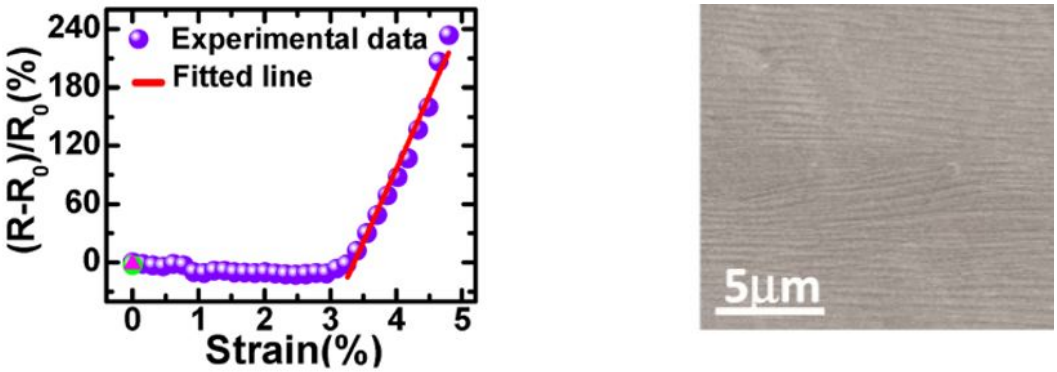

(a) Strain sensing **(b)** SEM image

Figure 2.3 Characterisation of Chemical Vapour Deposited graphene monolayer on a copper foil substrate [10]

In contrast to dry approaches, wet approaches refer to the deposition of graphene on a substrate from a solution and include processes such as ink-jet printing [4] [8], spray coating [17], drop-casting [11] and layer-by-layer self-assembly [20]. The resulting thin-films form connected networks that exhibit strain sensing properties through the change in contact resistance between connected flakes and tunneling effect between adjacent flakes [20]. The highest sensitivities reported so far used a layer-by-layer self-assembly technique with functionalised graphene nanoplatelets [20]. The reported gauge factor was as high as 1100. This high performance was attributed to the high uniformity of the deposited layer. Wet approaches can be used on irregular and rough substrates, as this research used graphene

coatings to measure strain variation on the surface of a light bulb [17], which may allow the printing of graphene on rough substrates such as cement.

2.2.2 Effect of Uniformity

Uniformity of graphene layers shows a strong correlation with the efficiency of the obtained sensing materials, with more uniform layers produced through layer-by-layer self-assembly showing higher sensitivities. [33]

Uniformity is influenced by the deposition techniques employed. Chemical deposition techniques, such as layer-by-layer self-assembly, exploit the chemical bonds between flakes and create uniformly arranged films [20]. On the other hand, drop-casting, spin coating, and ink-jet printing form networks of flakes with an arrangement dictated by the drying patterns of the ink on the substrate. Figure 4.2 clearly shows the variation in surface morphology of thin-film graphene materials. A drop-casted ink presents a high concentration of graphene on the perimeter, as shown in figure 2.4. This is attributed to the so-called "coffee-ring effect" that occurs when a solute deposits from an evaporating solvent. [2] Spin coating presents improved performance, while layer-by-layer self-assembly shows a more uniform film as presented in Figure 2.4 (f).

To improve the uniformity of the ink-jet printing processes, authors have tried to manipulate the ink properties by using dispersing agents [8] or by treatment of the substrate. [30] These methods have proved successful in reducing the sheet resistance of the obtained layer and achieving more dispersed thin-films. Therefore, the uniformity of the obtained graphene will be carefully studied in this research as a fundamental parameter for obtaining sensitive skins.

2.2.3 Effect of Sheet Resistance

Sheet resistance is a parameter that characterises how easy it is for electrons to flow through a thin film. It is expressed in $\Omega/\square$ (ohms per square), a measurement unit independent on the surface of the film. This measurement can be used to compare thin-films of the same uniform thickness, but not materials with different thicknesses.

An increased number of deposited graphene flakes create a gradually denser network.

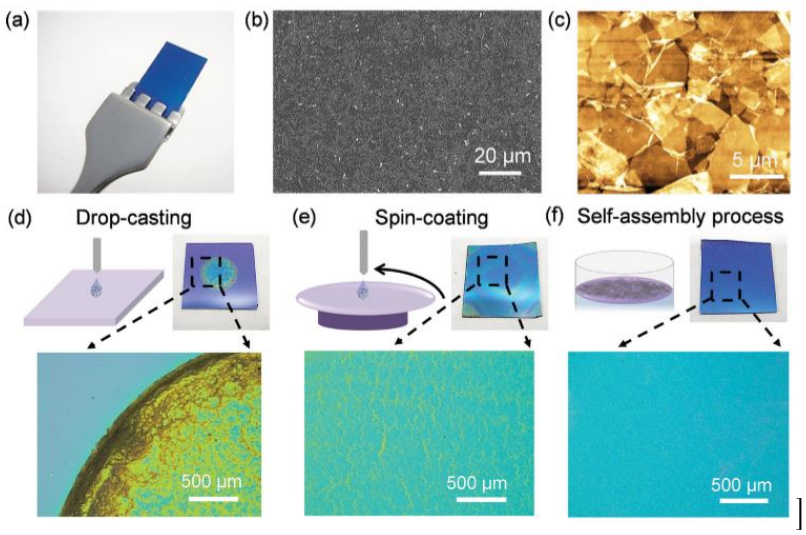

Figure 2.4 Characterisation of graphene films [20] (a) Photograph of ultrathin graphene films (UGF) deposited on a Si substrate. (b) SEM image and (c) AFM image of assembled UGF. (d) Drop-casting, (e) spin-coating, and (f) self-assembly processes for the production of graphene films

Lower sheet resistances are achieved with a higher number of deposited layers, at the expense of additional material deposition. The percolation threshold is defined as the required graphene quantity to obtain a sudden drop in sheet resistance. Figure 2.5 shows the typical behaviour of graphene sheet resistance with an increasing number of layers. When a low number of layers is deposited, a high resistance of $6500k\Omega/\square$ is recorded. This decreases gradually with an increasing number of deposited layers and reaches a resistance of $400k\Omega/\square$ for a fully percolated network. The sheet resistance of a thin film also increases if deposited on a non-conductive substrate. [19] The value of the percolation threshold depends both on the ink used and on the substrate. Because having a conductive network is a key requirement for self-sensing, this report will investigate the exact concentration of graphene required to reach percolation on the cement surface.

2.2.4 Effect of Sensing Mechanism

A contradiction is reported in the literature on whether lower sheet resistance of the printed graphene leads to higher or lower gauge factors. Sheet resistance is strongly correlated with the quantity of graphene deposited. Therefore, the correlation between sheet resistance and

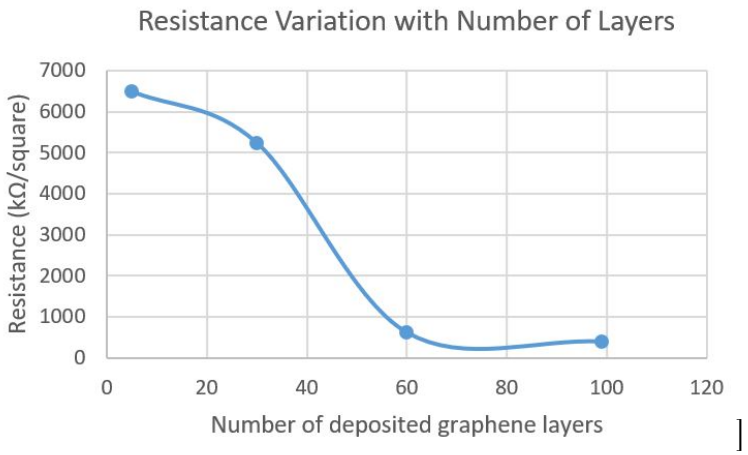

]

Figure 2.5 The percolation threshold of ink-jet printed graphene films adapted from [4]

gauge factor can be indicative of the correlation between material quantity and gauge factor.

On one hand, high sheet resistance is considered to lead to high sensitivities [17]. Figure 2.6b outlines the reported characteristic of gauge factor variation with sheet resistance. For a resistance of 10 $k\Omega$ up to a resistance of $10^5 k\Omega$, the gauge factor increases linearly from 10 to 150, on a logarithmic scale. This implies that less material is required to create conductive films and is attributed to charge transport in percolative graphene networks. The strain sensing mechanism is modelled as interconnected flakes that change their contact area with strain. Increased strain leads to increased distance between flakes and consequently to breakage of conductive paths. A network with higher resistance has less conductive paths. Therefore, the breakage of a single path leads to a higher fractional change in resistance, which would imply that less percolated networks have higher sensitivities.

On the other hand, gauge factor is reported to increase with lower sheet resistances [4]. Figure 2.6a (b) outlines the variation of the gauge factor with resistance, which presents a minimum at $10^5\Omega$. With resistances below this point, the gauge factor appeared to increase significantly, reaching a maximum value of 125 in the low resistance region. In the high resistance region, a mild increase in the gauge factor was observed with increased resistance. The nonlinear characteristic of the gauge factor versus resistance could be attributed to a change in sensing mechanism for more versus less percolated thin films, although the theoretical instrument for modelling the interactions of such flakes is still subject to research

[21].

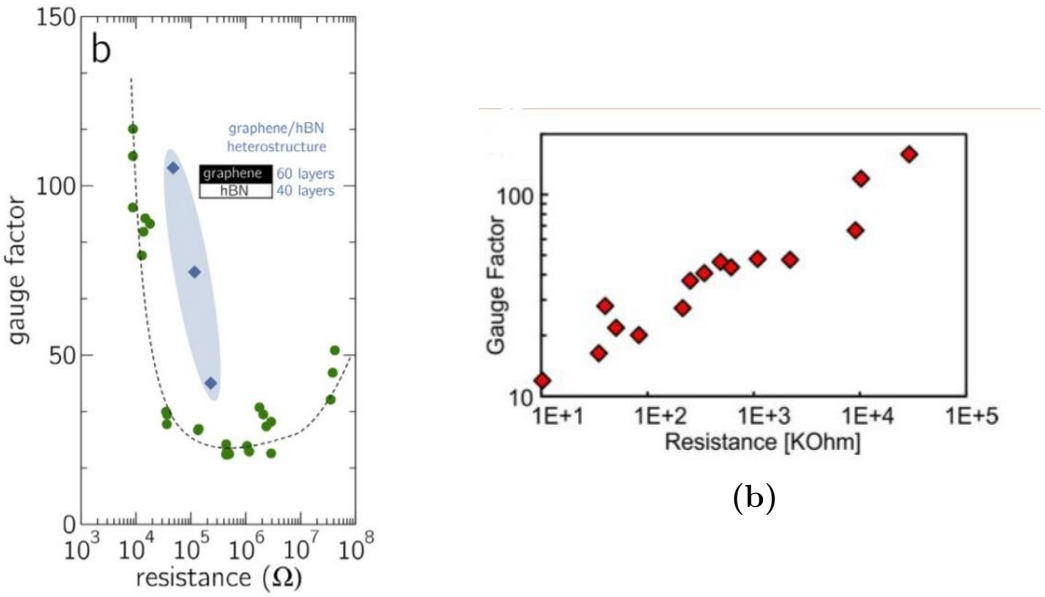

Figure 2.6 Variation of gauge factor with resistance for a) Ink-jet printed graphene films [4] and b) Spray-coated graphene networks [17]

An example of such a theoretical model describes the behaviour of graphene flakes sliding across each other [21]. The model analyses the conductive graphene flakes as they slide. It assumes that the sensing mechanism is based on the conductive path length variation between flakes that are in contact with each other. This leads to an estimated maximum gauge factor of 3, which is much lower compared to experimental data obtained for sliding graphene flakes. The simplifying assumptions behind this model, especially the exclusion of the tunneling effect from the equation and considering only the mechanical sliding between flakes as a source of strain sensing is considered as the reason for obtaining gauge factors that are close to the values of conventional metallic strain gauges, that do not present quantum tunneling between flakes. Therefore, quantum mechanical effects influence the strain sensing capabilities of graphene networks.

The disagreement in literature around whether a higher number of layers leads to improved or reduced sensitivity requires further experimental testing to establish, especially to correlate it to the optimal material quantity required for good sensitivity.

Chapter Three

MATERIALS AND METHODS

This chapter introduces the research materials used and methodology followed in this project and outlines what experimental methods were employed to obtain the desired data. The methods used are critically assessed against possible alternatives and reasoning provided for the chosen methodology.

3.1 Materials and Sample Preparation

In this research the materials used were graphene and cement. Graphene ink with 0.1 wt% solid contents, 3-4 cP viscosity in water solvent supplied by Cambridge Graphene [12] was used. The ink contained few-layer graphene with a lateral size of 80-500 nm, thickness smaller than 3 nm, and a graphene content of 0.2-0.5 mg/mL. Alcohol-based ink with few-layer graphene with a lateral size of 80-500 nm and a graphene concentration of 1.05 mg/mL was used. Table 3.1 outlines the properties of the ink used in the experiments. Portland Cement CEM I (52.5 N) supplied by Hanson Heidelberg Cement Group, produced according to BS EN 197-2 [28], was used.

Cubic and prismatic cement paste samples were prepared. The samples were made using cement and water with a water to cement ratio of 0.45, as a typical composition. The resulting paste was poured into moulds, cylindrical of 10 mm height and 50 mm diameter (Figure 3.1a) and prismatic of 20x30x15 mm (Figure 3.1b), in two layers, compacted and vibrated for 25 seconds to reduce entrapped air, then left for 24 hours with a polyethylene film at room temperature to prevent loss of moisture. After the specimens had hardened,

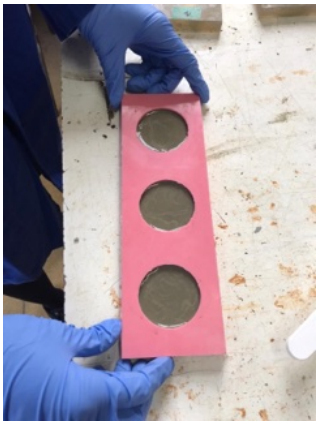

(a) Cylindrical Mould

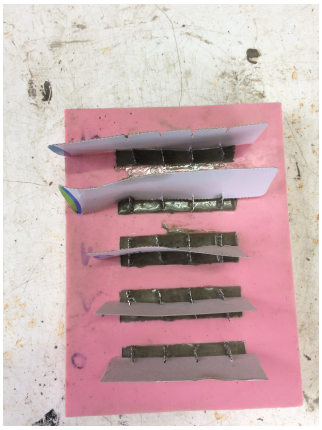

(b) Prismatic Moulds

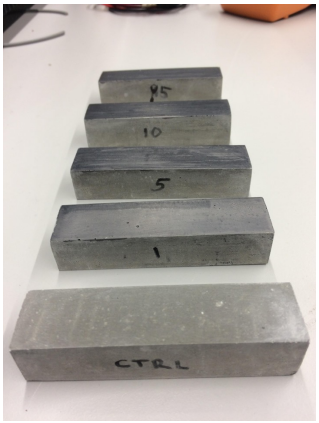

(c) Prismatic Samples

(d) Cubic Samples

(e) Water-based ink

(f) Alcohol-based ink

(g) Deposition process

Figure 3.1 Cement samples preparation process a) Mixer used for cement and water mixing b) Cylindrical moulds of 50 mm diameter and 10 mm thickness c) Prismatic moulds of 20 mm × 30 mm × 15 mm d) Cubic samples prepared from cutting the cylindrical samples e) Prismatic samples prepared f) Prismatic samples g) Alcohol-based deposition h) Deposition method

Characteristic	Graphink 1	Graphink 2
Solvent	Water	Alcohol
Viscosity (@ 100 s^{-1})	3-4 cP	-
Solids Content	0.1 wt%	-
Flake Type	Few-layer graphene	Few-layer graphene
Lateral size	80-500 nm	80-500 nm
Thickness	< 3 nm	< 3 nm
Graphene Content	0.2-0.5 mg/mL	1.05** mg/mL

Table 3.1 Mechanical and chemical properties of the graphene inks supplied by Cambridge Graphene [12]

the moulds were removed, specimens were cured in water at a temperature of 20 °C ± 2 °C. The cylindrical moulds were subsequently cut into 10x10 mm cubic samples, as shown in Figure 3.1d.

3.2 Research Methodology

Experimental procedures and measurements were planned to investigate the potential of graphene as a sensing coating for cement. The experiments were divided into three main areas: uniformity, conductivity, and self-sensing.

- **Uniformity**: understand the factors influencing the deposition of the graphene ink on the cement surface. Ink characteristics and environmental drying conditions were investigated. Scanning Electron Microscopy (SEM) and Energy-Dispersing X-Ray Spectroscopy (EDX) were used to assess the surface morphology

- **Conductivity**: correlate deposition parameters, such as ink type and the number of applied layers, to the final resistance of the obtained coating. Four-probe method sheet resistance measurements were used to measure sheet resistance.

- **Self-sensing**: characterise the sensing behaviour of the graphene-cement composite. The fractional change in resistance versus strain was analysed under three-point bending.

	Experiment		
	Self-Sensing	Self-Sensing	Self-Sensing
Sample Dimensions	Cube 10x10x10 (mm)	Cube 10x10x10 (mm) Prism 20x80x15 (mm)	Prism 20x80x15 (mm)
Curing	7 days	7 days	7 days
Mix Design	0.45 wt% w/c Ratio	0.45 wt% w/c Ratio	0.45 wt% w/c Ratio
Coating	Water-based ink (Graphink 1) Alcohol-based Ink (Graphink 2)	Water-based Ink (Graphink 2) Alcohol-based Ink (Graphink 2)	Alcohol-based Ink (Graphink 2)
Drying	Air Drying High Humidity Drying	Air Drying High Humidity Drying	Air Drying
Investigations	Scanning Electron Microscopy (SEM) Energy-Dispersing X-Ray Spectroscopy (EDS)	Four-Probe Measurement	Three-Point Bending Four-Probe Measurement
Measured Data	Surface Morphology Carbon Concentration on Surface	Sheet Resistance	Sheet Resistance Applied Load, Central Deflection

Table 3.2 Research Methodology

Three separate series of experiments were designed, as outlined in Table 3.2. First, the uniformity test experiments were conducted using cubic samples with water-based and alcohol-based inks. Second, conductivity properties were evaluated using the four-probe method on both the cubic samples and the prismatic samples, covered with alcohol-based ink and water-based ink. Third, three-point bending tests were conducted using alcohol-based ink only because it has a higher concentration of graphene and thus provided lower resistances. Specific procedures for graphene deposition, resistance measurement, and three-point bending test are detailed in the sections below.

3.3 Graphene Deposition

Graphene deposition was conducted using a syringe within a fume chamber environment. Two distinct types of graphene inks were deposited on the rough surface of cement, namely a water-based ink and an alcohol-based ink. Details of the chemical composition of each ink have been outlined in Table 3.1 which can be consulted for reference. The aim of the deposition stage was that, upon evaporation of the solvent from the surface, a conductive

and uniform coating of graphene to be obtained.

First, the water-based ink was deposited at room temperature. One layer was applied to the surface, left to dry for two hours, then followed by the deposition of another layer, as shown in Figures 3.1 f)-h). The square samples were covered with one, five, and ten graphene ink layers. Second, the water-based ink was deposited in a high-humidity environment under a controlled temperature of 20 °C and ± 2 °C, which led to a reduced evaporation rate of the water solvent. Therefore, the drying of the ink in a high-humidity environment had a duration of approximately four hours. Third, the alcohol-based graphene ink was deposited. This ink had the quickest evaporation rate of all the deposited specimens. Each layer was left to dry for 1 minute at room temperature before a second ink layer was applied.

The reason for using this deposition method for graphene is that it provided the ability to control the deposited pattern while having a similar strain-sensing mechanism as other wet approaches based on few-layer graphene, such as ink-jet printing. The inks used, supplied by Cambridge Graphene, are available in mass production and have the potential to extend into ink-jet printing. The application with a syringe does not exactly simulate an ink-jet printing process, but it has similar free variables such as the number of applied ink layers. The limitations of this method compared to other possible methods are that drying patterns for the deposition may be more pronounced.

3.4 Resistance Measurement

The electrical resistance of a material is defined as the ratio between the voltage V and a current I: $R = \frac{V}{I}$. When the resistivity ρ is wanted then a geometrical factor depending on the size and shape of the sample must be taken into consideration [13]. The resistivity is given by:

$$\rho = G \times \frac{V}{I} \tag{3.1}$$

where G is a geometrical factor related to the sample size and the electrode placement, V is the measured voltage and I is the current passed through the sample. The sheet resistance

is a convenient measure that characterizes thin-film materials and is given by:

$$R_s = \frac{\rho}{t} \tag{3.2}$$

where ρ is the resistivity and t is the thickness of the sheet. In this work, the value of t corresponds to the thickness of the applied graphene layer.

3.4.1 Two-probe Method

The two-probe method involves using only two electrodes for both injecting the current and measuring the voltage. When the value of the contact resistance and the resistance of the sheet are close, which is often the case for thin films as presented in this experiment, the contact probes can have a significant impact on the value of the measured sheet resistance. To prevent this, it is therefore desirable to separate the voltage and current electrodes, as it is achieved in the four-probe method described in the section below.

3.4.2 Four-probe Method

The four-probe method implies measuring sheet resistance using four electrodes. Two electrodes are used for injecting the current into the sample and the other two for measuring the voltage drop across the central region of the sample. Figure 3.3b outlines a typical set-up of the four-probe method. The final value of the sheet resistance for thin, rectangular sheets is calculated as follows:

$$R_s = \frac{\pi}{ln2} \times S(\frac{b}{s}, \frac{a}{b}) \times \frac{V}{I} \tag{3.3}$$

where the factor $\frac{\pi}{ln2}$ is a geometry factor corresponding to an infinitely large sheet of thickness t « s, and $S(\frac{b}{s}, \frac{a}{b})$ is an additional correction factor due to the finite, rectangular shape of the measured sample 3.2. The spacing between the measurement probes s, and the dimensions of the sample are known constants in the experiment and therefore the geometry factor can be easily calculated.

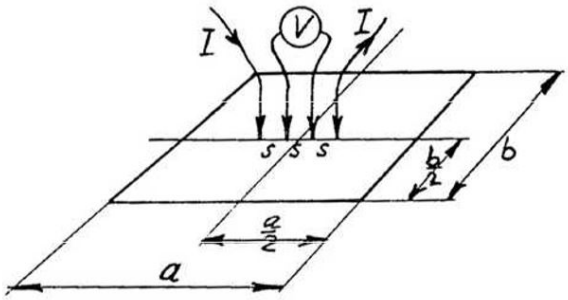

Figure 3.2 Four-Probe Method for Rectangular Thin Sheet [13]

3.4.3 Experimental Apparatus

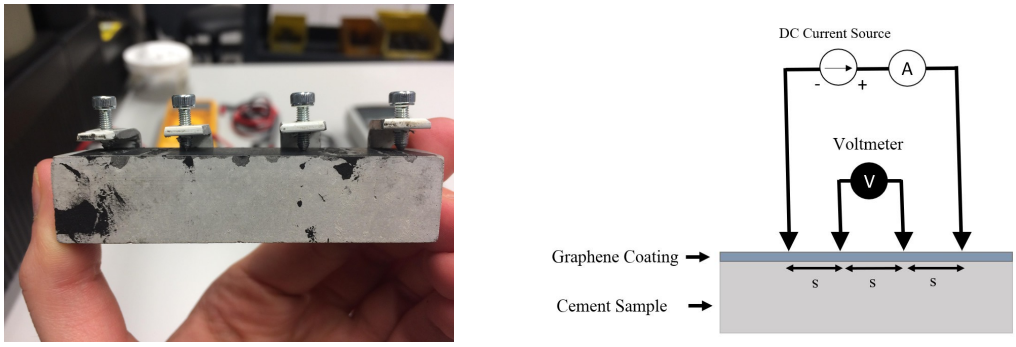

(a) Apparatus **(b)** Set-up diagram

Figure 3.3 Four-probe method set-up for measurement of graphene-cement composite with a) Physical apparatus and b) Diagram of measurement set-up

The sheet resistance was measured with an apparatus with four pointy electrodes placed in contact with the surface, as shown in Figure 3.3a. The probes were equally spaced at a distance s equal to 23 mm, as presented in Figure 3.3b. The geometry factor for resistance estimation from the voltage and current measurements was calculated according to section 3.4.2. The dimensions of the samples were a = 80 mm and b = 20 mm which results in $\frac{L}{b} = 4$ and $\frac{b}{s} = 0.8696$. This gives $S(\frac{b}{s}, \frac{a}{b}) = 0.2205$ and an overall geometry factor G = 0.9994. An ohm-meter was connected to the two central probes in parallel and the voltage measured. The current was measured in series from the outermost probes using a digital multimeter. The sheet resistance was finally calculated by using the following formula:

$$R_s = 0.9994 \times \frac{V}{I} \tag{3.4}$$

Alternative electrodes to the designed four-point apparatus were copper wire and silver paste electrodes, attached to the surface of the sample, or electrodes embedded into the cement paste. However, copper wire and silver paste electrodes caused graphene delamination and were challenging to install, while embedded electrodes measured the resistance of the underlying cement paste, rather than the resistance of the coating. Compared to these alternatives, pointy electrodes provided the most reliable results and thus were selected for the final experiment.

3.5 Three-point Bending Test

The three-point bending test was used to characterise the self-sensing behaviour of the composite by correlating the change in strain of the specimen with the measured change in sheet resistance of the applied graphene layer. Linear elasticity was assumed for the material, which permitted the calculation of flexural strain, ϵ, and stress, σ, at the midspan, M, of the cement sample, given the central vertical displacement, δ:

$$\epsilon_f = \frac{6d\delta}{L^2} \tag{3.5}$$

$$\sigma = \frac{FLd}{8I} \tag{3.6}$$

where L is the length of the specimen, d is the depth of the beam, F is the force applied by the load cell nose, and I is the second moment of area for the specimen. Figure 3.4 shows a schematic of the experimental set-up. The flexural strain and stress are calculated at point M, the midspan of the tension side of the specimen.

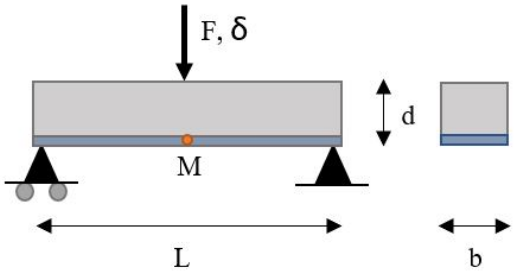

Figure 3.4 Diagram of experimental set-up for three-point bending test

An Instron Electromechanical UTS 2kN machine as shown in Figure 3.5a was used to perform the three-point bending test was performed in load control, with the force F increasing in steps of 10 N. The failure load of one control specimen was recorded, with all subsequent samples loaded to 60% of the maximum strength. At each step the applied load F, central deflection of the beam δ, injected current I, and voltage drop V were recorded. The sheet resistance was then measured indirectly by using equation 3.4 and the measured values of I and V. The positioning of the four-probe apparatus is shown in Figure 3.5b.

(a) Instron UTS 2kN Machine

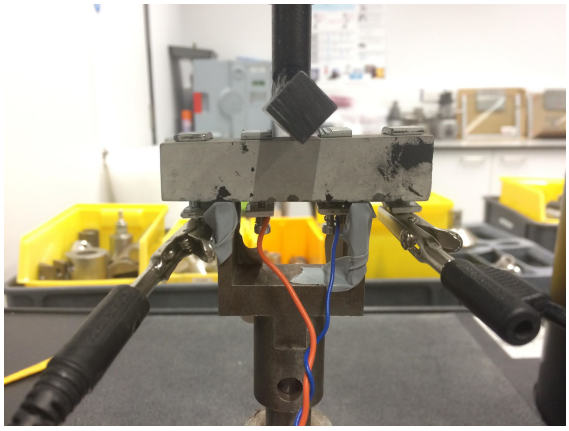

(b) Four-probe apparatus

Figure 3.5 Experimental set-up for three-point bending test

3.6 Scanning Electron Microscopy

The Scanning Electron Microscope (SEM) instrument used to obtain images of the graphene flakes deposited on the cement surface and undertake energy-dispersing X-ray Spectroscopy (EDS) analysis, was a ZEISS EVO LS 15, shown in Figure 3.6. Square cement samples were placed in a vacuum chamber for 24h and examined under an 8kV accelerating voltage.

Figure 3.6 ZEISS EVO LS 15 scanning electron microscope (SEM) used for investigating the surface morphology of the specimens

Chapter Four

Results and Discussion

This chapter outlines the main findings of the project. It presents an analysis of the experimental results and compares them to the literature, as well as assessing the performance of the coating compared to existent alternatives.

4.1 Uniformity of the graphene coating

Uniformity of deposited particles, namely the spatial arrangement of few-layer graphene flakes on the sample surface subsequent to solvent evaporation, is a key parameter studied to characterise graphene-cement sensors. Different deposition techniques and drying environments compatible with cement sample fabrication are investigated and compared.

4.1.1 The "coffee-ring" effect

Initial experiments involved the deposition of water-based graphene ink on the cement sample surface at room temperature. The drying pattern was investigated under the Scanning Electron Microscope (SEM) to understand the characteristics of the obtained coating. Following water evaporation, the deposition pattern showed regions of high graphene concentration on the sample edge, leaving the central region completely uncovered. This characteristic was depicted under SEM, as narrow stripes of conductive graphene flakes were noticeable on the sample edge, but not in the centre. Figure 4.1 outlines the obtained surface images from SEM both in the central region and in the edge regions of the sample, which show an increase

in graphene concentration with an increased number of deposited layers, as expected. For one layer in the centre of the sample, the surface morphology shows just pristine cement. For ten layers a higher concentration of deposited graphene flakes is apparent, as suggested by the lighter stripes on the surface profile.

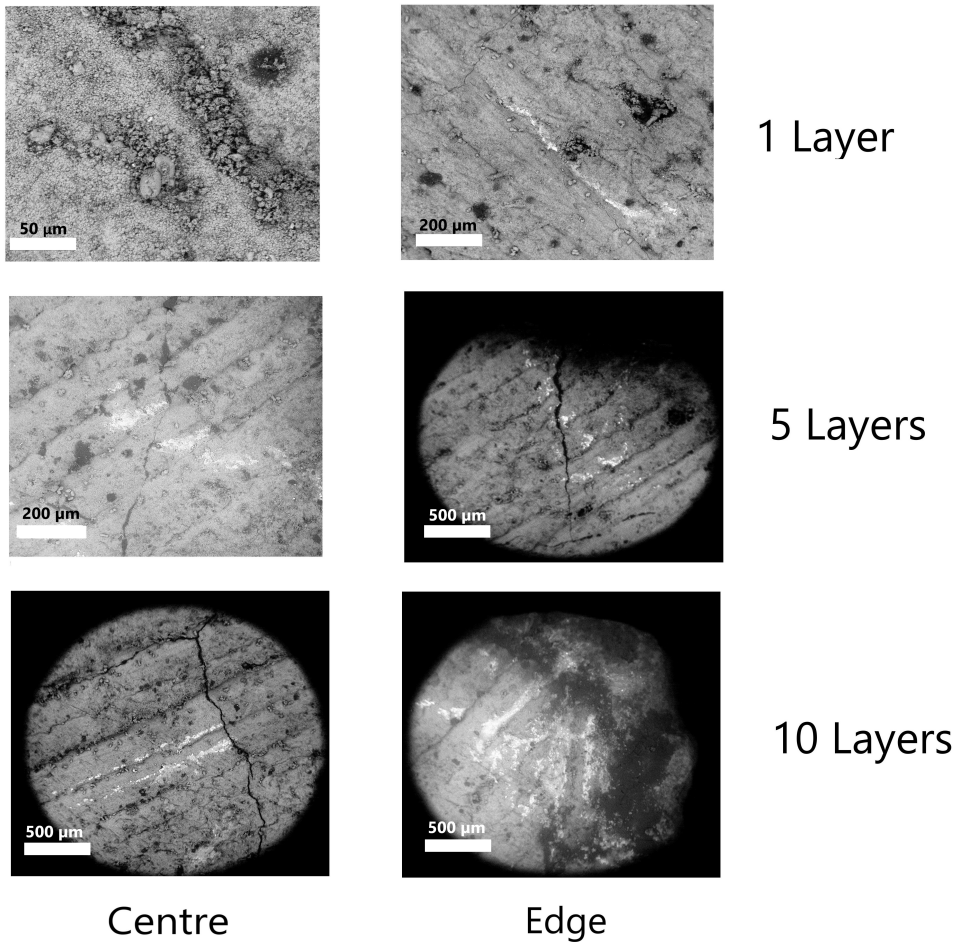

Figure 4.1 SEM images of initial samples with 1, 5, 10 layers of graphene ink drying in air at room temperature where the images on the left are for the centre region of the sample and the image on the right are for the edge of the sample

The ink was found to be uniformly distributed on the entire surface at deposition time, but after solvent evaporation, only stripes along the perimeter of the square were observed to be conductive. The central region of the cement sample had the same resistance as the control cement paste, which is in the order of 10^6 $k\Omega$, as tested by a two-probe method. However, the region on the sample perimeter had a resistance almost three orders of magnitude lower,

indicating that the deposited graphene flakes formed a conductive path on the edge of the sample, but not in the centre. Small individual flakes migrated within the ink solvent during the evaporation process. This behaviour was an indication of the so-called "coffee ring effect".

When a droplet of ink containing dispersed particles dries on a surface, it often leaves a ring-like deposit along its perimeter. This so-called "coffee-ring effect" is governed by the transport of the solute inside the solvent during evaporation [7]. The dimensionless Peclet number can be used to examine the ratio of advection to diffusion as a transport mechanism for the solute, $Pe = \frac{J_0 L}{D}$, where J_0 is the evaporation rate, L is the size of the droplet and D is the diffusion coefficient. In general, $Pe >> 1$ indicates that the advective transport dominates whereas $Pe << 1$ diffusion is the dominant mechanism [2]. A more homogeneous deposit would be expected when diffusion dominates the flow. Therefore, increasing the humidity of the environment and thus lowering the evaporation rate would lead to a more uniform particle distribution.

4.1.2 Drying conditions

To investigate the impact of the drying conditions on the deposition pattern of the graphene inks and to characterise the properties of the resulting surface, samples coated with alcohol-based ink and water-based ink were left to dry in both air and in a high-humidity environment. The concentration of deposited graphene flakes on the edge and in the central region of the sample is shown in Figure 4.2. The figure shows the variation in carbon concentration with the number of applied ink layers, for both the alcohol-based ink, as well as for the water-based ink. As expected, concentrations are higher on the edge of the sample than in the centre, due to the "coffee-ring effect". To quantify the effect, the maximum difference in concentration between the central region of the sample and the edge region at a specific number of deposited layers is chosen as a figure of merit. This is maximum for the alcohol-based ink at five number of layers being 12%. This figure is smaller for the water-based ink, at only 4.98% for ten layers of ink, indicating a relatively more uniform deposition. Thus, reduction in the evaporation rate of the solvent by controlling the environmental conditions of the drying process could improve the uniformity of the obtained layer, as theoretically

predicted [2]. Notably, one layer of alcohol-based ink dried within one minute, compared to one layer of water-based ink that dried within 4 hours in a high-humidity environment. Thus alcohol-based inks showed good dry time compared to water-based inks, at the expense of reduced uniformity. To sum up, this experiment shows that the uniformity of the deposited graphene layer could be controlled by varying the environmental drying conditions of the material. Successfuldeposition of graphene ink on the cement substrate is demonstrated.

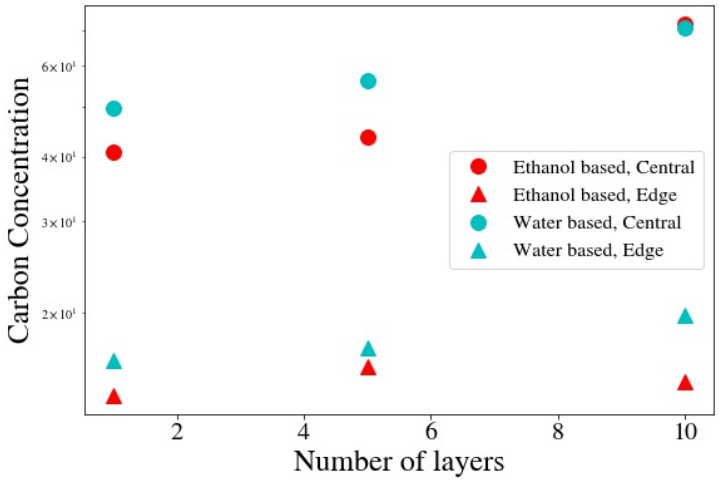

Figure 4.2 Uniformity of the deposited graphene layers on the edge and centre regions of the samples tested

4.1.3 Surface morphology

The surface morphology of the coated graphene-cement composite is studied to assess the uniformity and deposition pattern of the few-layer graphene on the surface. For the water-based ink, calcium carbonate ($CaCO_3$) crystals formed on the surface of the sample due to the reaction of the water (H_2O) inside the ink with carbon dioxide (CO_2) and calcium oxide (CaO) in the cement paste. The series of chemical reactions are shown below:

$$CaO + H_2O \rightarrow Ca(OH)_2 \tag{4.1}$$

$$Ca(OH)_2 + CO_2 \rightarrow CaCO_3 + H_2O \tag{4.2}$$

SEM images confirm the formation of calcite, as presented in Figure 4.3. The surface characteristic appears dominated by the CO_3 deposition. The morphology seems uniform across both the central and the edge region. EDX was also used to identify the elemental composition of the scanned surfaces. Graphene is an allotrope of carbon and therefore high carbon concentration on the sample indicates the presence of graphene flakes on the surface. The elemental composition obtained for the deposition of water-based ink confirms the CO_3 formation on the surface. It is reported that for one layer of deposited ink the detected elements include: 51.42% oxygen, 30.83% calcium and 13% carbon. Therefore, the formation of calcium carbonate dominates the surface morphology of the water-based ink coated specimen.

For the alcohol-based ink, the conductive graphene characteristic is shown in the SEM image of Figure 4.4. Clearly identifiable graphene flakes are deposited on the surface, as highlighted in the light regions of the image. This means that during the quick-drying process of the alcohol-based ink on the surface, small droplets and non-uniformities in the ink deposition directly translate into graphene flake patterns on the surface. The elemental composition of the scanned samples shows a 40.95% carbon concentration on the surface, which indicates successful graphene deposition.

To sum up the uniformity investigations, the surface morphology of water-based inks shows a more uniform deposition, achieved by reducing the evaporation rate through drying in a high-humidity environment. The carbon concentration deposited on the cement substrate, of 13%, is, however, low for enabling self-sensing properties. Thus, even though deposition in a high humidity environment is observed as being effective for reducing the coffee ring effect, further experiments are conducted using the alcohol-based ink, primarly for its good conductivity properties.

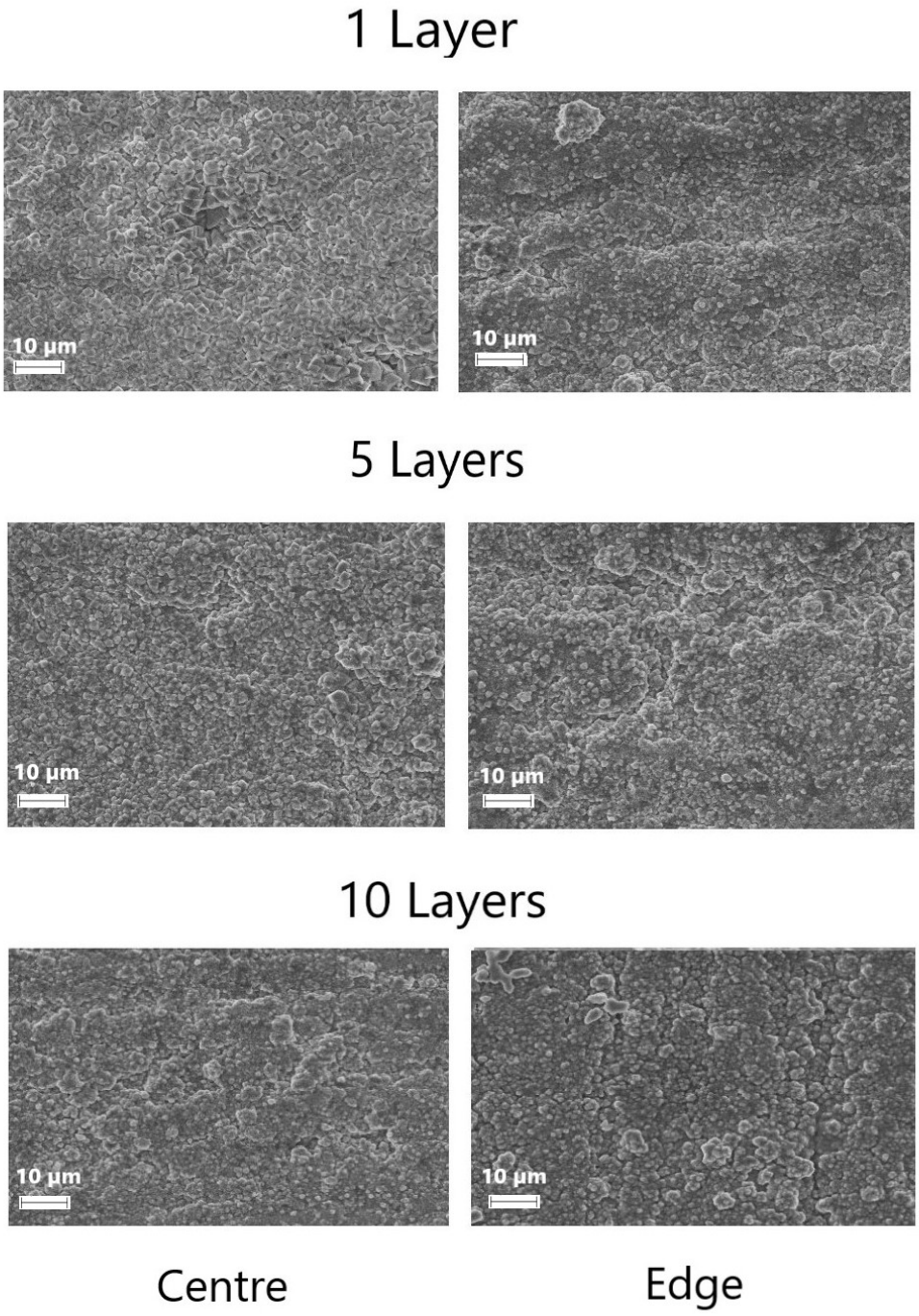

Figure 4.3 SEM images of samples coated with water-based ink and dried in a high-humidity environment where the images on the left are for the centre region of the sample and the image on the right are for the edge of the sample

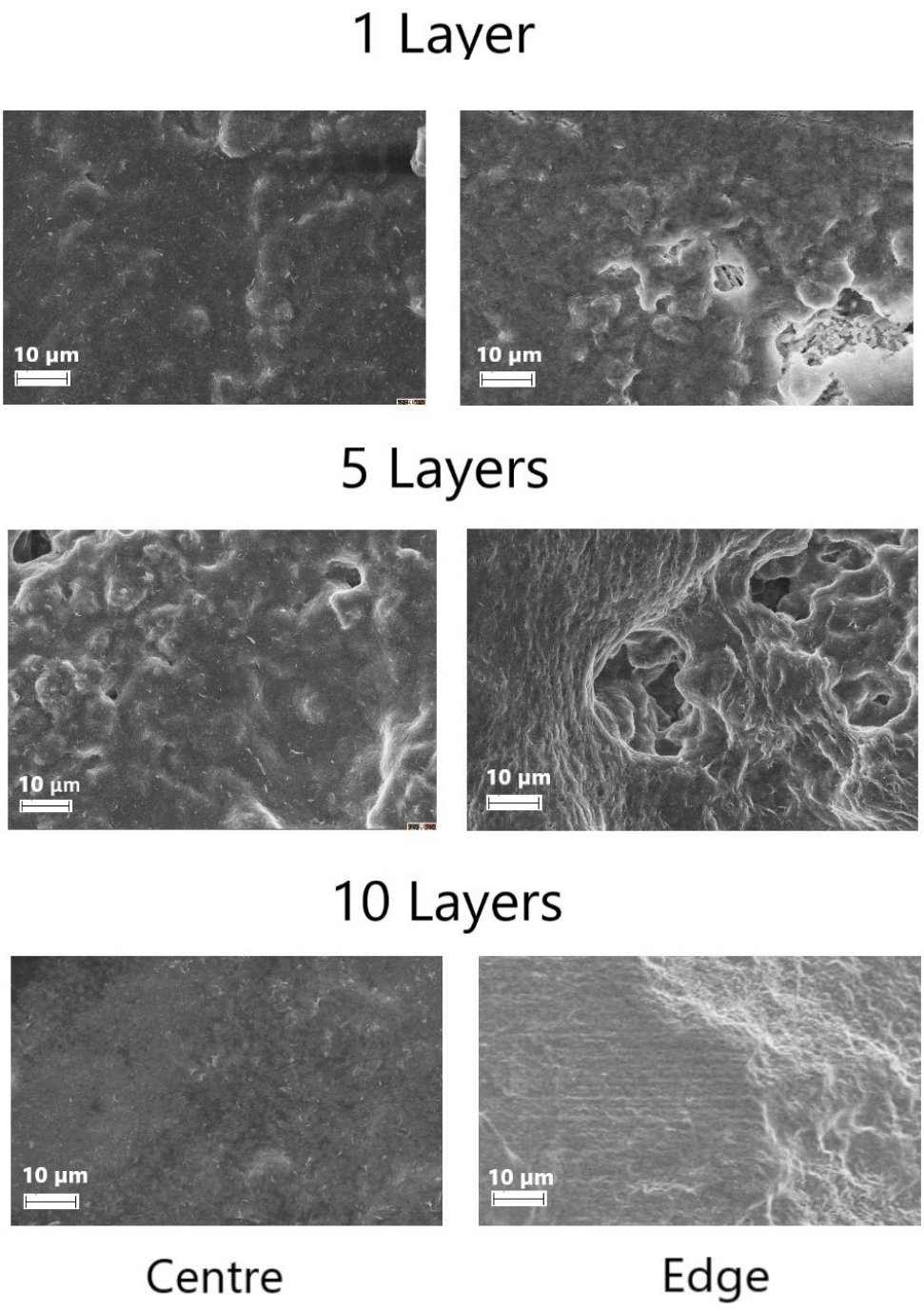

Figure 4.4 SEM images of samples coated with alcohol-based ink and dried at room temperature where the images on the left are for the centre region of the sample and the image on the right are for the edge of the sample

4.2 Conductivity

This section outlines the conductivity properties of deposited graphene flakes on the cement surface. The conductivity is characterised by the sheet resistance of the applied graphene layers. In this section one layer of graphene refers to one layer of ink deposited on the surface, rather than one monolayer graphene sheet. This nomenclature will be consistent throughout the section.

4.2.1 Sheet Resistance

Sheet resistance appears to decrease with an increasing number of graphene layers. This result is expected based on the percolation theory, which suggests the decrease in resistance follows a second-order decay [30]. The phenomenon is clearly illustrated in Figure 4.5. Initially the sheet resistance is relatively high at 16 k$\Omega/\square$, but it decreases gradually with an increasing number of layers to 0.81 k$\Omega/\square$. As higher graphene quantities are deposited on the substrate, the flakes form conductive, connected networks. Percolation occurs when five ink layers are applied, which corresponds to a quantity of 5.25 mg of few-layer graphene. To aid in comparison, the data collected from our experiment is plotted against data reported by other authors. This shows a similar trend of high initial resistance, followed by a sudden drop and then saturation. Both presented results, the literature, and this study use ink-printed few-layer graphene. In literature, it is common to refer to the point where significant conductivity change occurs as the percolation threshold of the material.

4.2.2 Percolation Threshold

The percolation threshold is defined as the concentration of particles required on a surface to reach a sudden drop in resistance. Achieving a conductive network is important in self-sensing applications. This section presents the estimated quantity of graphene required to reach percolation on the cement surface.

In this set of experiments the sheet resistance data was analysed in comparison to the carbon concentration deposited on the surface. Carbon concentration was considered an

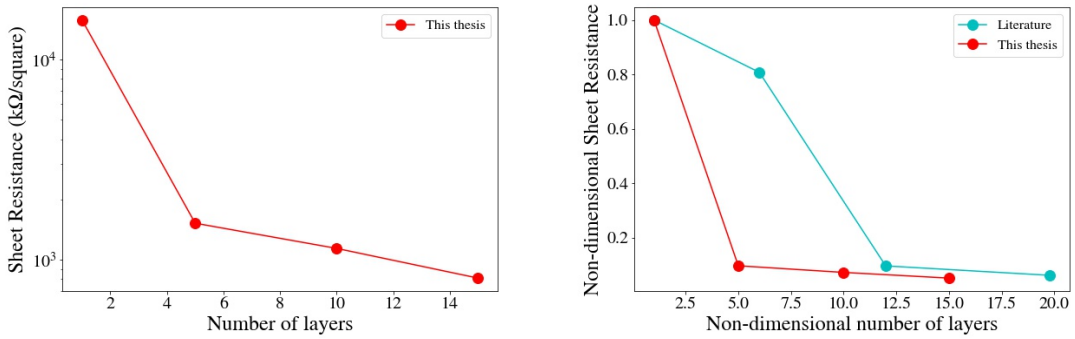

(a) (b)

Figure 4.5 Reduction in sheet resistance with an increased number of layers for a) Own experimental data and b) Non-dimensional comparison with the literature in ref [4]

alternative representation to the number of deposited layers, with the advantage that it directly relates to the flake distribution on the surface. Figure 4.6 outlines the variation in sheet resistance with the carbon concentration on the sample surface. The sheet resistance appears to follow an inverse relationship to the carbon concentration. In the top left corner of the image, the red data points correspond to the water-based ink samples. Samples appear to have a resistance that is close to that of control cement, at 10^6 $k\Omega$. In the bottom right corner, the blue points correspond to the alcohol-based ink. The alcohol-based ink shows a gradually decreasing trend in resistance with carbon concentration. Overall, at around 50% carbon concentration a drop in sheet resistance is observed, which is attributed to the percolation threshold.

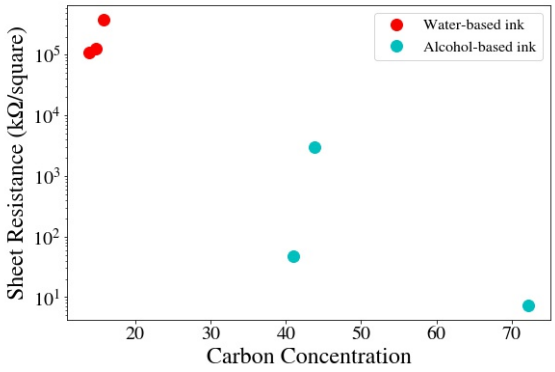

Figure 4.6 Conductivity variation with carbon concentration

This result can be explained with the percolation theory. The percolation theory says that the occupation probability required for an infinite network to form on a 2d square sample such as the one in our experiment is 1/2 [5]. This means that from the sites available on the cement sample 50% need to be occupied for a conductive network to form. This is what the results of this experiment show, that when the concentration of carbon on the surface reaches 50% a drop in resistance occurs due to the ability of the flakes to connect in a network. As the network becomes more dense the resistance continues to drop at a slower rate. When the surface of the sample reaches a 100% occupation with flakes, there is marginal benefit in increasing the deposited quantity of material as the resistance drop for further material deposited becomes insignificant.

This result has engineering significance because it means that the deposited graphene quantity on the surface can be optimized to suit the needs of the designed sensors. Conductive coatings can, therefore, be designed with a carbon concentration of only 50% on the surface, reducing the cost of manufacturing and the required material.

4.3 Self-Sensing

Self-sensing refers to the ability of the deposited graphene layer to sense changes in the strain of the concrete sample. This section outlines the progress made towards developing a graphene sensing skin.

4.3.1 Stress-strain Characteristic

In three-point bending, the graphene-cement samples deform and become internally stressed due to the applied load. The linear elastic assumptions, namely assuming infinitesimal strains, a linear stress-strain curve, and no material yield, allows for the calculation of the relationship between vertical displacement and flexural strain, as described in detail in Equation 3.6. For a brittle material, such as the cement samples, these assumptions are expected to be an accurate representation of the real material behaviour. The stress-strain response of the cement samples depends on the stiffness and strength of the graphene-

cement composite. At seven days curing the cement-based material is brittle. This section presents the response of the graphene-cement composite to loading and discusses the validity of the linear-elastic assumptions. Stiffness improvements through graphene coating are also outlined.

Initial testing up to failure of a control sample without graphene coating registered a flexural strength of 10.93 MPa. The fracture surface of the specimen indicated brittle fracture, with a crack occurring at the midspan, as shown in Figure 4.7.

Figure 4.7 Fracture surface of the control sample

Subsequent specimens were loaded up to approximately 60% of the failure load to ensure operation in the linear regime. The stress-strain characteristic showed a linear correlation between stress and strain, as expected, except for an initial strain offset caused by the positioning of the loading nose on the cement sample surface at the onset of the test. The raw data obtained is displayed in Figure 4.8a, where the effect of bedding errors is present. At the start of the experiment, the loading nose of the three-point bending machine did not reach full contact with the specimen surface. As the loading nose was moving downwards, an increase in vertical displacement was recorded. This displacement, however, did not correspond to actual strain in the cement specimen. The flexural strain was calculated using linear-elastic equations from the vertical displacement of the loading nose, as described by Equation 3.6. Thus, the calculated flexural strain was higher compared to the actual value recorded in the material. The as-measured strains were processed to remove the offset by extrapolating the

linear region of the stress-strain curve and subtracting the x-axis intercept. This operation resulted in the stress-strain characteristic shown in Figure 4.8b. Stress increases linearly with strain and the measured strains are in the order of $\mu\epsilon$, with no yield being apparent. Thus, the linear-elastic assumption is confirmed for the composite.

Figure 4.8b not only shows the linear relationship between stress and strain but also the stiffness of the graphene-cement composite as the slope of the graph. In the figure, there is an increase in slope between the samples with one, five, ten, and fifteen layers of the applied coating. Graphene flakes applied on the tension side of the specimen present slight reinforcement, with an escalation in stiffness being apparent amongst the tested samples. Young's modulus increases from a value of 2.691 GPa for the sample with one layer of applied graphene to 4.63 GPa for the sample with fifteen layers of applied graphene. Comparing this result to literature, for a cement paste sample with a w/c ratio of 0.45 and 7 days of curing, the reported Young's Modulus was 14 GPa [9]. This indicates a lower Young's Modulus of the obtained samples than the literature suggests.

In summary, linear-elastic assumption is confirmed for the graphene-cement composite. The cement samples have a flexural strength of 10.93 MPa in the absence of coating and a Young's Modulus between 2.69 GPa and 4.63 GPa, which is lower compared to the literature, but the stiffness increases with an increasing number of deposited graphene layers amongst the tested samples.

4.3.2 Sensing Mechanism

Self-sensing relies on the change in resistance with a variation in strain of the composite. The sensing skin was coated on the tension side of the sample and therefore subjected to positive strain. The change in resistance recorded in the sheet due to the applied strain is reported in this section. Initial readings in the sheet resistance variation versus strain indicate an offset between the resistance of the one-layer graphene and the resistance of the fifteen-layer graphene samples, as shown in Figure 4.9a. The resistance versus strain relationships appear straight due to the large difference between their mean recorded values.

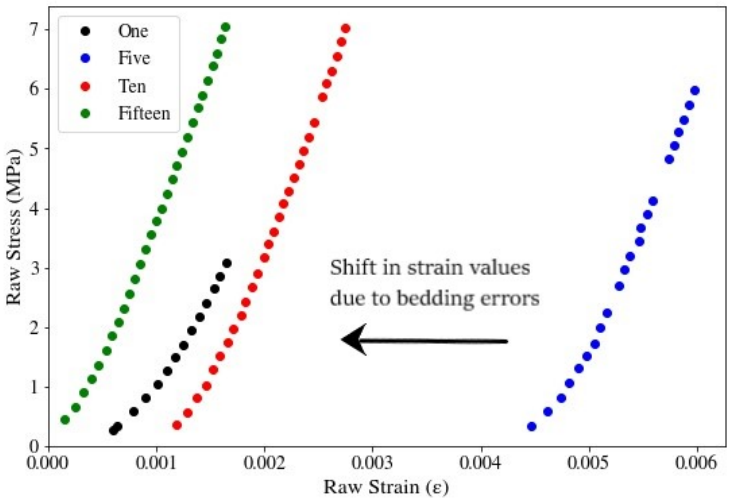

(a) As measured

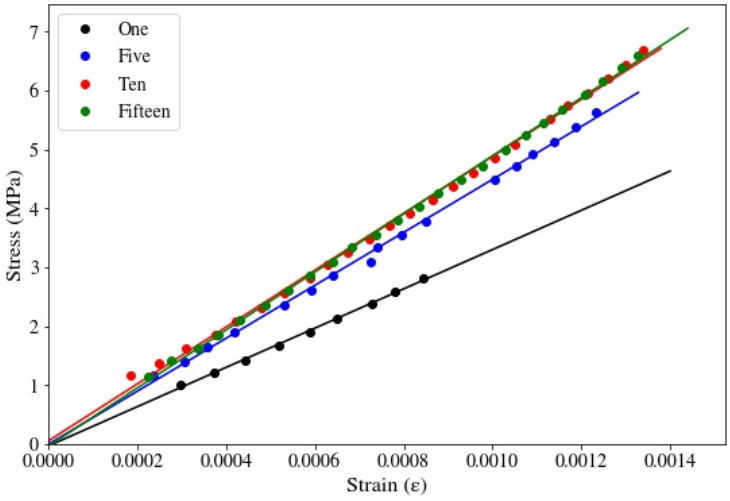

(b) Linear stress-strain relationship

Figure 4.8 Stress-strain relationship in the graphene-cement composite for a) Raw measured data and b) Processed data to remove bedding errors shows a linear-elastic behaviour of the composite for the tested strains

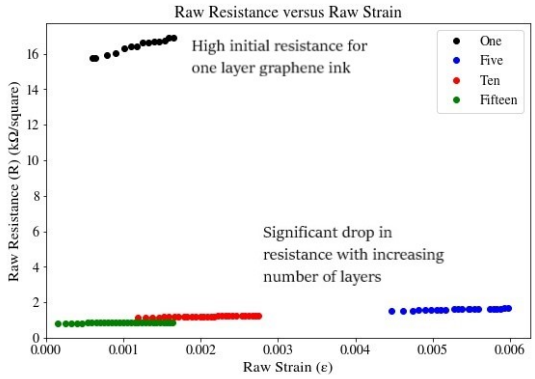

(a) As measured

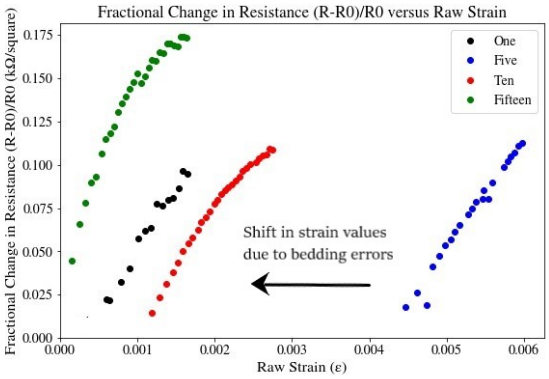

(b) Non-dimensional resistance

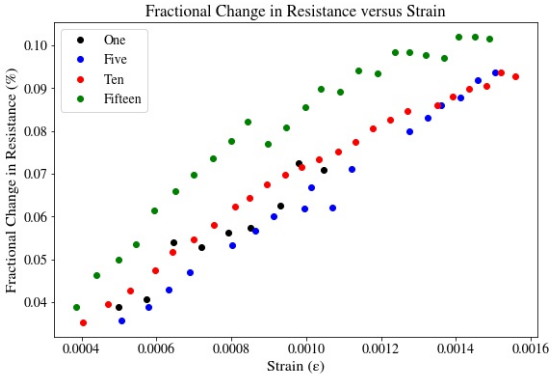

(c) Non-dimensional resistance versus Strain

Figure 4.9 Self-sensing mechanism of the graphene-cement composite as described by the fractional change in resistance versus strain with a) Raw measurements b) Fractional change in resistance versus raw strains c) Fractional change in resistance versus strain

This behaviour is caused by the reduction in resistance of the sheet with an increasing number of ink layers deposited on the surface. This is in agreement with the results presented previously in Figure 4.5. The high difference in initial sheet resistance between the experimental samples prohibits a direct comparison of their sensing properties by analysing the raw data. Therefore, a non-dimensional representation of the sheet resistance is required, in the form of Fractional Change in Resistance (FCR).

In the next stage, the FCR is calculated as $FCR = (R - R_0)/R_0$ and plotted against the raw strains, as shown in Figure 4.9b. The initial strain offset and the bedding errors are removed according to the methodology described in section 4.3.1., leading to a graph of FCR against the strain in the graphene-cement composite, presented in Figure 4.9c. Resistance increases with increasing tensile strain values. The slope of the fractional change in resistance versus strain graph is the Gauge Factor (GF) $GF = FCR/\epsilon$, a common figure of merit used in literature to describe the sensing performance of both strain sensors and self-sensing composites [1] [27] [2]. The green line shows the sensing behaviour of fifteen layers of applied ink. It presents a higher initial slope compared to the other samples, indicating that an increased graphene quantity may lead to better sensitivity. It also presents a non-linear profile in the strain regions above $80\mu\epsilon$. This behaviour is further characterised in section 4.3.3., where a linearising method is proposed for the sensing skin.

Comparing this result to literature, there is an agreement that the fractional change in resistance increases with increasing tensile strains. Graphene strain sensors present increasing resistance with increased strain [11] [10] [4] whereas carbon fiber coatings on cement surface also follow a similar characteristic [1].

The increase in resistance with increased strain is expected due to the breakage of conductive paths in the graphene flake network. The few-layer graphene on the cement surface come in close contact with each other, despite the roughness of the substrate. The contact resistance that forms between neighbouring graphene flakes, as well as the tunnelling current flowing between non-contact, but adjacent flakes, contributes to the creation of a percolative path for electron transport between the four electrodes. Due to the nano-scale size of the few-layer graphene applied on the surface, 3nm thick and less than 300nm in

lateral size, these flakes adhere to the cement substrate and mimic its mechanical movement [17]. In the event of concrete strain, the relative distance between flakes changes, which leads to variation in the contact resistance between flakes and a change in the path of charge transport between the electrodes. This translates into the strain-sensing response depicted in Figure 4.9c.

In summary, an increase in fractional change in resistance and strain are correlated, which suggests that few-layer graphene coatings can work as a strain sensor for a cement substrate. This is the first graphene-cement coating with proven strain sensing properties reported in the reviewed literature. Fifteen layers of graphene appear more sensitive to strain compared to one, five, and ten layers, but the non-linear effects are stronger in for a higher number of layers. This non-linear effect is discussed in the following section.

4.3.3 Linearity

This section investigates the linearity of the graphene-cement composite sensing system and shows a function that matches the experimental data. The sensitivity of the skin, as described by the gauge factor, is also discussed. It is important to point out that a second order polynomial relationship between the fractional change in resistance and the applied strain is observed. The increase in resistance weakens for higher strain values, as shown in Figures 4.10a-4.10d. The experimental observation is mathematically modelled with a second-order function and the Fractional Change in Resistance (FCR) becomes, as a function of strain:

$$FCR(\epsilon) = A\epsilon^2 + B\epsilon + C \tag{4.3}$$

where ϵ is the strain measured in the experiments and A, B and C are parameters to be fitted onto the measured data. Solving the simple second-order equation for ϵ, gives a unique solution for estimated flexural strain, by setting the condition for $\epsilon > 0$:

$$\epsilon_{estimated} = \frac{-B + \sqrt{B^2 - (4AC - FCR)}}{2A} \tag{4.4}$$

Performing a second-order polynomial regression on the data, parameters A, B, C can be

Second-order fit coefficients				
No. Layers	A	B	C	R^2
1	-33903.5	112.09	-0.0095	0.956
5	562.13	58.32	0.0047	0.995
10	-23693	97.03	-0.001	0.999
15	-52492	154.00	0.0071	0.99

Table 4.1 Second-order fit coefficients for fractional change is resistance versus strain data

calculated for each set of samples one to fifteen. The parameters A, B, C obtained for each sample are shown in Table 4.1, alongside the determination coefficients R^2. Quantitatively, the coefficients indicate a high degree of determination (>0.95) between the estimated second-order function and the measured data. The second-order model appears to accurately depict the sensing characteristic of the sample for the given strain range.

The strain-dependent GF that characterises the sensitivity of the graphene-cement composite can be calculated as the rate of change in FCR with ϵ:

$$GF = \frac{\partial FCR(\epsilon)}{\partial \epsilon} = 2A\epsilon + B \tag{4.5}$$

Higher gauge factors are indicative of higher sensitivity. The gauge factor thus depends linearly on the strain, ϵ. This behaviour is clearly outlined in Figure 4.11. Fifteen layers of applied graphene ink present a linear variation in the gauge factor between 154 at 20 $\mu\epsilon$ and 19.3 at 130 $\mu\epsilon$. Similarly, ten layers of applied ink present a variation between 80 at 20 $\mu\epsilon$ to 35 at 140 $\mu\epsilon$. Five layers of applied ink show a perfectly constant gauge factor of 61 across all strains. Therefore, the deposited graphene quantity on the surface influences the sensitivity and linearity of the graphene-cement composite. A comparison of the second-order fit for all strain values is shown in Figure 4.10e. The improved linearity of the response could be because five deposited layers of graphene ink correspond exactly to the percolation threshold. It was shown in Section 4.2.2, Figure 4.5 that a significant drop in resistance occurs when five layers of graphene ink are applied on the surface. The quantity of graphene deposited is 5.25 mg, as obtained by depositing five layers, 1 mL each, with alcohol-based graphene ink of concentration 1.05 mg/mL. If less graphene than the percolation threshold

is deposited, the response presents a scattered profile, as it is the case for one layer of applied graphene ink. On the other hand, if the percolation threshold is exceeded, as it is the case for ten and fifteen layers of graphene ink applied on the surface, the response starts to behave non-linearly due to overlapping graphene flakes sliding across each other. Thus, for optimal linearity this thesis suggests that a quantity of graphene equal to the percolation threshold, 5.25 mg, should be deposited on the surface, namely five layers of graphene ink.

Compared to literature, the values of the GF are within the reported range. Ink-jet printed graphene coatings on paper have a reported GF of 125 [4] that is constant across all reported strains. Higher gauge factors are reported by [20] who uses a layer-by-layer self-assembly method for the deposition of thin-films and reports variations in the gauge factor with strain, correlated to an exponential increase in GF due to increasing strain associated with a stronger breakage of graphene paths [20].

In summary, the graphene-cement composite presents a second-order electrical response to the applied strain. The response is influenced by the number of applied graphene layers, with a higher number of layers presenting reduced linearity, but better sensitivity. For only five layers of applied graphene ink or 5.25 mg of graphene, linear response with a constant GF across all strains of 61 is obtained.

4.3.4 Failure Detection, Repeatability, and Fatigue

The experiments planned to assess the failure detection, repeatability, and fatigue resistance of the graphene-cement composite were interrupted due to the Cambridge University closure in light of the COVID-19 pandemic. The expected results are outlined in this section. Failure detection was to be investigated by loading the samples to fracture, to 410 N based on the control sample. A sharp increase in sheet resistance was expected upon failure, due to the fracture of the sensitive coating and breakage of the conductive paths [31]. Repeatability and fatigue results were expected to identify whether the graphene coating undergoes structural damage upon deformation. Further details are provided in Appendix 2.

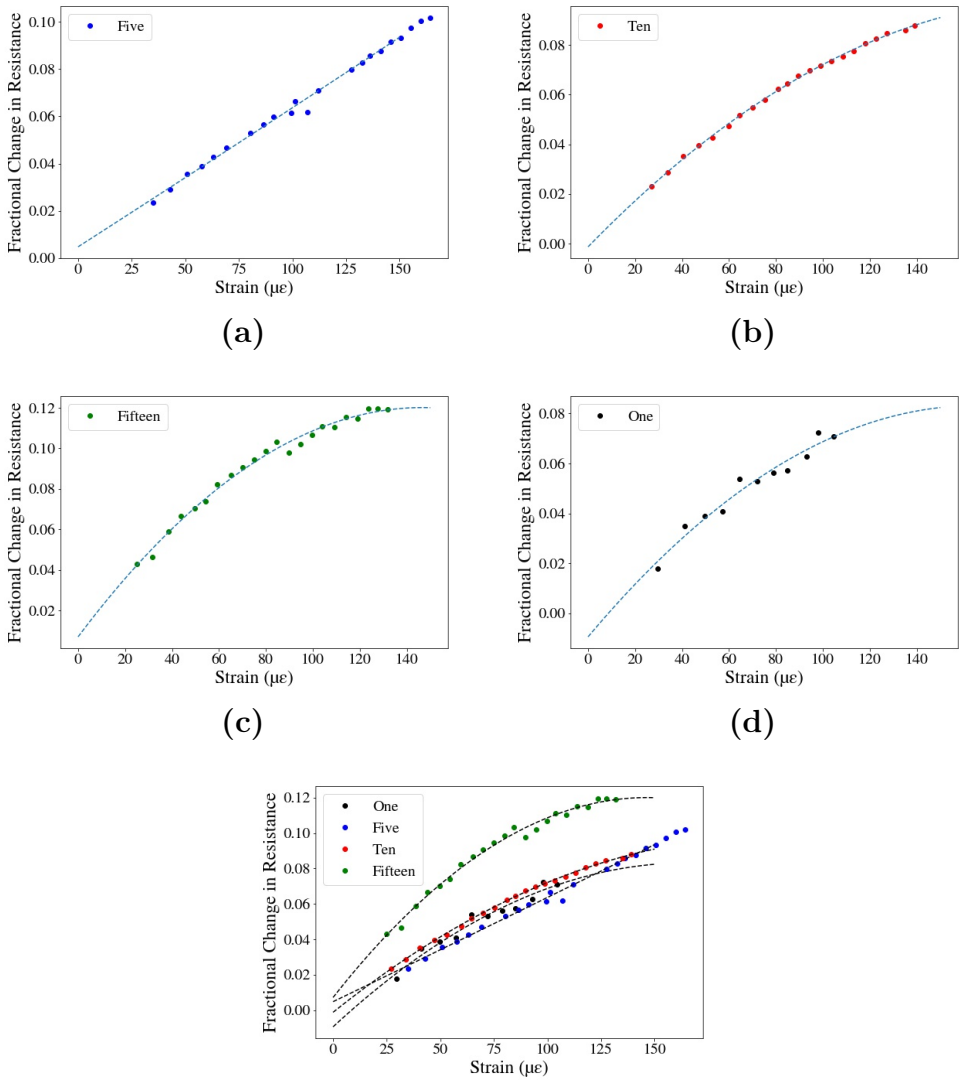

Figure 4.10 Measured fractional change in resistance versus strain with second order fit a) One layer b) Five layers c) Ten layers and d) Fifteen layers e) All layers

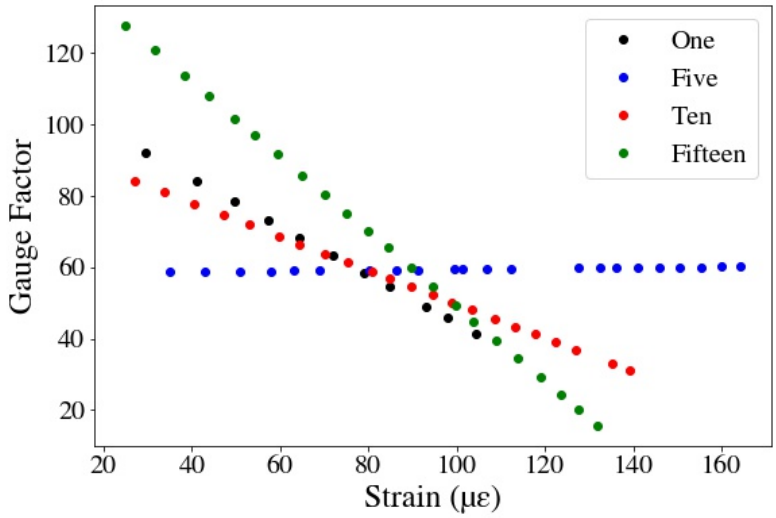

Figure 4.11 Gauge factor variation with the applied strain for one, five, ten and fifteen layers of applied graphene flakes on the surface

Chapter Five

Conclusions

This thesis initiated the development of an all-graphene sensing skin for cementitious materials. Through literature review, experimental planning and results analysis, a graphene-cement coating was developed. Project objectives were achieved as far as establishing the impact of graphene on the uniformity and resistivity of the surface, developing an experimental methodology and assessing the self-sensing capabilities of the material. The sensitivity properties of the skin were characterised in terms of the fractional change in resistance versus strain response.

The literature review identified key issues in the deposition of graphene on a cement substrate. First, the type of graphene used and the deposition method influenced the properties of the resulting film. Monolayer graphene deposited via Chemical Vapour Deposition presented the formation on wrinkles on the surface, which made it unsuitable for deposition on a cement substrate. Few-layer graphene in a low-boiling point solvent ink, such as water or alcohol, presented challenges in deposition related to the "coffee-ring effect". Therefore, experimental procedures were targeted to reduce this effect. Second, to minimise the quantity of graphene required for obtaining a conductive coating, the relationship between the number of applied graphene layers and the sensitivity of the resulting coating were investigated. A contradiction was found in literature on whether increasing the quantity of deposited material leads to higher or lower gauge factors.

The experimental work used a deposition of few-layers graphene ink on the cementitious substrate. Investigations were conducted on uniformity, conductivity, and self-sensing. The number of applied graphene layers was the free variable for optimising the thickness of the

resulting coating. Investigations conducted include SEM, resistance measurement, and three-point bending test. Pointy electrodes were used to measure the value of the sheet resistance as they were shown more reliable compared to alternatives such as copper electrodes or embedded electrodes.

The results showed that a more uniform deposition and a reduction of the so-called "coffee-ring effect" can be achieved by drying the samples in a high humidity environment. The alcohol-based ink showed short dry-times of approximately one minute, whereas the water-based ink in a high-humidity environment dried within four hours. The conductivity properties of the cement-graphene coatings were shown to improve with increased addition of graphene on the cement substrate. The percolation threshold was recorded at 50% carbon on the cement surface. The stress versus strain response showed a slight increase in the stiffness of the composite with the addition of the graphene layer, from 2.691 GPa to 4.63 GPa. This value was lower compared to the literature but an increase between coated and non-coated samples was observed. The sensing capabilities of the skin were confirmed, with strains as low as 20 $\mu\epsilon$ being detected. The graphene-cement composite presents a second-order response to the applied strain. A linear response was achieved at a deposited quantity of only 5 graphene ink layers, with a gauge factor of 61. This value corresponds to the percolation threshold of the graphene on the surface and therefore has high sensitivities. Limitations of the study include the followed deposition method which, although was effective in simulating certain aspects of ink-jet printing, led to the formation of drying patterns on the cement surface.

5.0.1 Future work

Future work to improve the properties of the coating could be focused on optimizing the deposition parameters. This thesis suggests a method for improving the uniformity of the layer, by manipulating the ink drying environment. However, approaches with a layer-by-layer self-assembly process to create a thin-film transferred onto the cement substrate could further improve sensing capabilities. Moreover, fatigue resistance, repeatability, and damage detection experiments were suspended due to University closure during the COVID-19 pandemic. This could form the basis of future experiments.

APPENDIX

.1 COVID-19 Implications

The University of Cambridge closure in light of COVID-19 led to several planned experiments not being conducted as scheduled. While the obtained results were considered insightful, and it was decided to present them in the obtained form, a list of further planned experiments is outlined below. This can be a basis for future work on the topic of self-sensing graphene materials. The purpose of the planned experiments was to further characterise the built sensor in terms of fatigue resistance, failure detection capabilities, and measurement repeatability.

	Experiment		
	Self-Sensing	Self-Sensing	Self-Sensing
Investigation	Three-Point Bending	Three-Point Bending	Three-Point Bending
Loading	Cyclic loading with 60% of failure load	Linear loading up to failure	Linear loading and unloading
Observation	Fatigue resistance	Failure detection mechanism	Repeatability
Date	13.03.2020	16.03.2020	17.03.2020

Figure 1 Experiments Influenced by COVID-19 University Closures

.2 Risk Assessment

In this section, a reflection on the suitability of the risk assessment conducted prior to the commencement of the project will be conducted. The Hazard Assessment conducted at the start of the year proved suitable for working with potentially hazardous substances in a laboratory environment that may present specific risks. The assessment of the suitability of the control measures is outlined in Table 1 below. The assessment of risk management measures shows that the undertaken steps were effective in preventing incidents. One measure proved to be cautious - wearing steel-toe cap boots in the laboratory environment - as it was proved to be a limited risk for dropping heavy objects in the lab. A future risk assessment should include more detailed instructions on the disposal of contaminated equipment such as syringes with graphene inks. In this project, the syringes were contained after use and disposed of with contaminated waste. Graphene deposition was conducted in a fume chamber environment, which is recommended for future experiments.

Hazard	Effect	Measure	Assessment
Dust	Respiratory disease	Approved Dust Mask	Effective
Foot Injury	Physical short-term injury	Steel Toe Cap Boots	Cautious
Flying Particles	Eye injury	Protective Goggles	Effective
Manual Handling	Spinal injury	Handling Techniques	Effective
Harmful Substances	Skin Disease, long-term illness	COSHH Assessment, protective gloves and lab coat to be worn at all times	Effective

Table 1 Risk Assessment

REFERENCES

[1] Francisco Javier Baeza et al. "Multifunctional cement composites strain and damage sensors applied on reinforced concrete (RC) structural elements". In: *Materials* 6.3 (2013), pp. 841–855. ISSN: 19961944. DOI: 10.3390/ma6030841.

[2] J. A. Barnard, H. Meloy Gorr, and J. Zueger. "Characteristic Size for Onset of Coffee-Ring Effect in Evaporating Lysozyme-Water Solution Droplets". In: *The Journal of Physical Chemistry* 116 (2012), pp. 12213–12220.

[3] Alexander Bessonov et al. "Highly reproducible printable graphite strain gauges for flexible devices". In: *Sensors and Actuators, A: Physical* (2014). ISSN: 09244247. DOI: 10.1016/j.sna.2013.11.034.

[4] C. Casiraghi and M. et al Macucci. "Inkjet printed 2D-crystal based strain gauges on paper". In: *Carbon* (2018). ISSN: 00086223. DOI: 10.1016/j.carbon.2017.12.030.

[5] Kim Christensen. *Percolation Theory*. Tech. rep. 2002.

[6] Sungwoo Chun, Yeonhoi Choi, and Wanjun Park. "All-graphene strain sensor on soft substrate". In: *Carbon* 116 (2017), pp. 753–759. ISSN: 00086223. DOI: 10.1016/j.carbon.2017.02.058. URL: http://dx.doi.org/10.1016/j.carbon.2017.02.058.

[7] R. Deegan et al. "Capillary Flow as the Cause of Ring Stains from Dried Liquids Drops". In: *Nature* 389 (1997), pp. 827–829.

[8] Lucja Dybowska-Sarapuk et al. "Efficient inkjet printing of graphene-based elements: Influence of dispersing agent on ink viscosity". In: *Nanomaterials* 8.8 (2018), pp. 9–14. ISSN: 20794991. DOI: 10.3390/nano8080602.

[9] R. F. Feldman and Huang Cheng-yi. "Properties of portland cement-silica fume pastes II. Mechanical properties". In: *Cement and Concrete Research* 15.6 (1985), pp. 943–952. ISSN: 00088846. DOI: 10.1016/0008-8846(85)90083-3.

[10] Xue Wen Fu et al. "Strain dependent resistance in chemical vapor deposition grown graphene". In: *Applied Physics Letters* 99.21 (2011), pp. 1–4. ISSN: 00036951. DOI: 10.1063/1.3663969.

[11] Mohammed Gamil et al. "Graphene-based strain gauge on a flexible substrate". In: *Sensors and Materials* 26.9 (2014), pp. 699–709. ISSN: 09144935. DOI: 10.18494/sam.2014.1030.

[12] Cambridge Graphene. "GRAPHINK 1 Safety Data Sheet GRAPHINK 1 Safety Data Sheet". In: 2006.1907 (2018), pp. 1–7.

[13] Haldor Topsoe. "Geometric factors in four-probe resistivity testing". In: *Bulletin No. 472* (1968).

[14] Milad Hallaji, Aku Seppänen, and Mohammad Pour-Ghaz. "Electrical impedance tomography-based sensing skin for quantitative imaging of damage in concrete". In: *Smart Materials and Structures* 23.8 (2014). ISSN: 1361665X. DOI: 10.1088/0964-1726/23/8/085001.

[15] Baoguo Han, Xun Yu, and Eil Kwon. "A self-sensing carbon nanotube/cement composite for traffic monitoring". In: *Nanotechnology* 20.44 (2009), p. 445501. ISSN: 0957-4484. DOI: 10.1088/0957-4484/20/44/445501.

[16] Baoguo Han, Liqing Zhang, and Jinping Ou. "Self-Sensing Concrete". In: *Smart and Multifunctional Concrete Toward Sustainable Infrastructures*. Singapore: Springer Singapore, 2017, pp. 81–116. ISBN: 978-981-10-4349-9. DOI: 10.1007/978-981-10-4349-9{_}6. URL: https://doi.org/10.1007/978-981-10-4349-9_6.

[17] Marek Hempel et al. "A novel class of strain gauges based on layered percolative films of 2D materials". In: *Nano Letters* 12.11 (2012), pp. 5714–5718. ISSN: 15306984. DOI: 10.1021/nl302959a.

[18] Yenny Hernandez et al. "High-yield production of graphene by liquid-phase exfoliation of graphite". In: *Nature Nanotechnology* 3.9 (2008), pp. 563–568. ISSN: 17483387. DOI: 10.1038/nnano.2008.215.

[19] Jiantong Li and Fei Ye. "Efficient inkjet printing of graphene". In: *Advanced Materials* 25.29 (2013), pp. 3985–3992. ISSN: 09359648. DOI: 10.1002/adma.201300361.

[20] Xinming Li et al. "Large-Area Ultrathin Graphene Films by Single-Step Marangoni Self-Assembly for Highly Sensitive Strain Sensing Application". In: *Advanced Functional Materials* 26.9 (2016), pp. 1322–1329. ISSN: 16163028. DOI: 10.1002/adfm.201504717.

[21] Zheng Li and Qing Sheng Yang. "Sensing mechanism of flexible and stretchable composites based on stacked graphene". In: *Materials and Design* 187 (2020), p. 108384. ISSN: 18734197. DOI: 10.1016/j.matdes.2019.108384. URL: https://doi.org/10.1016/j.matdes.2019.108384.

[22] Kenneth J. Loh et al. "Carbon nanotube sensing skins for spatial strain and impact damage identification". In: *Journal of Nondestructive Evaluation* 28.1 (2009), pp. 9–25. ISSN: 01959298. DOI: 10.1007/s10921-009-0043-y.

[23] Xiaocun Lu et al. "Autonomous Damage Detection in Multilayered Coatings via Integrated Aggregation-Induced Emission Luminogens". In: *ACS Applied Materials and Interfaces* 10.47 (2018), pp. 40361–40365. ISSN: 19448252. DOI: 10.1021/acsami.8b16454.

[24] Dimitrios G. Papageorgiou, Ian A. Kinloch, and Robert J. Young. "Mechanical properties of graphene and graphene-based nanocomposites". In: *Progress in Materials Science* 90 (2017), pp. 75–127. ISSN: 00796425. DOI: 10.1016/j.pmatsci.2017.07.004. URL: http://dx.doi.org/10.1016/j.pmatsci.2017.07.004.

[25] Ioanna Papanikolaou, Noemi Arena, and Abir Al-Tabbaa. "Graphene nanoplatelet reinforced concrete for self-sensing structures – A lifecycle assessment perspective". In: *Journal of Cleaner Production* (2019). ISSN: 09596526. DOI: 10.1016/j.jclepro.2019.118202.

[26] Sohel Rana et al. "A review on smart self-sensing composite materials for civil engineering applications". In: *AIMS Materials Science* 3.2 (2016), pp. 357–379. ISSN: 23720468. DOI: 10.3934/matersci.2016.2.357.

[27] Thomas Schumacher and Erik T. Thostenson. "Development of structural carbon nanotube-based sensing composites for concrete structures". In: *Journal of Intelligent Material Systems and Structures* 25.11 (2014), pp. 1331–1339. ISSN: 15308138. DOI: 10.1177/1045389X13505252.

[28] Technical Data Sheet. "Hanson Portland Cement". In: 2006.January (2020), pp. 4–5.

[29] Sandeep Sony, Shea Laventure, and Ayan Sadhu. "A literature review of next-generation smart sensing technology in structural health monitoring". In: *Structural Control and Health Monitoring* 26.3 (2019), pp. 1–22. ISSN: 15452263. DOI: 10.1002/stc.2321.

[30] Felice Torrisi and Tawfique et al Hasan. "Inkjet-printed graphene electronics". In: *ACS Nano* 6.4 (2012), pp. 2992–3006. ISSN: 19360851. DOI: 10.1021/nn2044609.

[31] Wei Wang, Hongzhe Dai, and Sigang Wu. "Mechanical behavior and electrical property of CFRC-strengthened RC beams under fatigue and monotonic loading". In: *Materials Science and Engineering A* 479.1-2 (2008), pp. 191–196. ISSN: 09215093. DOI: 10.1016/j.msea.2007.06.046.

[32] Peter Wick et al. "Classification framework for graphene-based materials". In: *Angewandte Chemie - International Edition* 53.30 (2014), pp. 7714–7718. ISSN: 15213773. DOI: 10.1002/anie.201403335.

[33] Min Juey Yee, N. M. Mubarak, and Abdullah et Al. "Carbon nanomaterials based films for strain sensing application—A review". In: *Nano-Structures and Nano-Objects* 18 (2019), p. 100312. ISSN: 2352507X. DOI: 10.1016/j.nanoso.2019.100312. URL: https://doi.org/10.1016/j.nanoso.2019.100312.